Article:
Coppola, D., Giordano, D., Milazzo, L. et al. (2018) Coexistence of multiple globin genes conferring protection against nitrosative stress to the Antarctic bacterium Pseudoalteromonas haloplanktis TAC125. Nitric Oxide, 73. pp. 39-51.

https://doi.org/10.1016/j.niox.2017.12.006

Coexistence of multiple globin genes conferring protection against nitrosative stress to the Antarctic bacterium *Pseudoalteromonas haloplanktis* TAC125

Daniela Coppola[a], Daniela Giordano[a,b], Lisa Milazzo[c], Barry D. Howes[c], Paolo Ascenzi[d], Guido di Prisco[a], Giulietta Smulevich[c], Robert K. Poole[e], Cinzia Verde[a,b,f*]

[a]*Institute of Biosciences and BioResources (IBBR), CNR, Via Pietro Castellino 111, I-80131 Naples, Italy*

[b]*Stazione Zoologica Anton Dohrn, Villa Comunale, Naples, Italy*

[c]*Department of Chemistry 'Ugo Schiff', University of Firenze, Via della Lastruccia 3-13, I-50019 Sesto Fiorentino (Fi), Italy*

[d]*Interdepartmental Laboratory for Electron Microscopy, Roma Tre University, Via della Vasca Navale 79, I-00146 Rome, Italy*

[e]*Department of Molecular Biology & Biotechnology, The University of Sheffield, S10 2TN, UK*

[f]*Department of Biology, Viale Marconi 448, Roma Tre University, I-00146 Rome, Italy*

***Running title**: The role of bacterial globins in the Antarctic environment*

[*]**Corresponding author:**

Cinzia Verde

E-mail: c.verde@ibp.cnr.it; cinzia.verde@ibbr.cnr.it

Abstract

Despite the large number of globins recently discovered in bacteria, our knowledge of their physiological functions is restricted to only a few examples. In the microbial world, globins appear to perform multiple roles in addition to the reversible binding of oxygen; all these functions are attributable to the heme pocket that dominates functional properties. Resistance to nitrosative stress and involvement in oxygen chemistry seem to be the most prevalent functions for bacterial globins, although the number of globins for which functional roles have been studied *via* mutation and genetic complementation is very limited. The acquisition of structural information has considerably outpaced the physiological and molecular characterisation of these proteins.

The genome of the Antarctic cold-adapted bacterium *Pseudoalteromonas haloplanktis* TAC125 (*Ph*TAC125) contains genes encoding three distinct single-chain 2/2 globins, supporting the hypothesis of their crucial involvement in a number of functions, including protection against oxidative and nitrosative stress in the cold and O_2-rich environment. In the genome of *Ph*TAC125, the genes encoding 2/2 globins are constitutively transcribed, thus suggesting that these globins are not functionally redundant in their physiological function in *Ph*TAC125. In the present study, the physiological role of one of the 2/2 globins, *Ph*-2/2HbO-2217, was investigated by integrating *in vivo* and *in vitro* results. This role includes the involvement in the detoxification of reactive nitrogen and O_2 species including NO by developing two *in vivo* and *in vitro* models to highlight the protective role of *Ph*-2/2HbO-2217 against reactive nitrogen species. The *PSHAa2217* gene was cloned and over-expressed in the flavohemoglobin-deficient mutant of *Escherichia coli* and the growth properties and O_2 uptake in the presence of NO of the mutant carrying the *PSHAa2217* gene were analysed. The ferric form of *Ph*-2/2HbO-2217 is able to catalyse peroxynitrite isomerisation in vitro, indicating its potential role in the scavenging of reactive nitrogen species. Here we present *in vitro* evidence for the detoxification of NO by *Ph*-2/2HbO-2217.

Keywords: Antarctic cold-adapted bacterium; bacterial globin; nitrosative/oxidative stress; Resonance Raman spectroscopy.

1. Introduction

Many bacterial genomes contain genes encoding more than a single globin and there is a strong correlation between the number of globin genes and the genome size (Giovannoni et al., 2005). Globins are classified in three families: (*i*) myoglobin (Mb)-like proteins (M), displaying the classical three-on-three (3/3) α-helical sandwich motif; (*ii*) sensor globins (S), and (*iii*) truncated (T) hemoglobins (Hbs), showing the two-on-two (2/2) α-helical-sandwich motif (Vinogradov et al., 2013). Members of the T family (also known as 2/2Hbs) are found in eubacteria, cyanobacteria, protozoa, and plants, but not in animals (Wittenberg et al., 2002; Milani et al., 2005; Vinogradov et al., 2013). On the basis of phylogenetic analysis, the T family can be further divided into three distinct sub-families/groups: HbI (or N), HbII (or O) and HbIII (or P), with a novel, small (4%) clade of sequences named HbIV (or Q) that contains only bacterial sequences (Bustamante et al., 2016).

Some of the organisms hosting the 2/2Hbs are pathogenic bacteria; others perform photosynthesis, fix nitrogen or may display distinctive metabolic capabilities (Pesce et al., 2013, and refs therein). Some proposed functions include protection from reactive oxygen and nitrogen species (ROS and RNS, respectively), O_2 and sulfide chemistry (Pesce et al., 2013, and refs therein; Boubeta et al., 2016). In fact, recent genome analyses (Vinogradov et al., 2013; Bustamante et al., 2016) reveal a preponderance of 2/2Hbs in cyanobacteria and green algae, and phylogeny supports the rise of these globins after the appearance of life about 3 billion years ago (Vinogradov et al., 2006). Since the 2/2Hbs scaffold probably evolved before the development of the current aerobic environment, a putative original role for these proteins could have been that of O_2 detoxification following the increase of O_2 levels and the evolution of photosynthesis (Crowe et al., 2013). The search for globin physiological functions is further driven by the evidence that many 2/2Hbs are capable of reacting with NO, nitrite, and peroxynitrite (Gardner, 2005; Ascenzi et al., 2009; De Marinis et al., 2009; Ascenzi et al., 2014; Pesce et al., 2016). Interestingly, an unusual occurrence of the concomitant presence of 2/2Hbs of group II and flavohemoglobin (FHb) in the same genome

has been demonstrated (Vinogradov et al., 2013). These findings might indicate that the function of the 2/2Hbs of group II can be intimately linked to the well-known function of FHb in NO detoxification (Gardner et al., 1998; Membrillo-Hernàndez et al., 1999; Mills et al., 2001; Stevanin et al., 2000). In some cases, 2/2Hbs from more than one group can coexist in the same organism, indicating diversification of their functions (Vinogradov et al., 2013). The 2/2Hbs have amino-acid sequences either shorter or longer than those of α and β globins and Mb (i.e. less than 130 and more than 160 residues, respectively).

The most striking differences between the 2/2 and the 3/3 globin folds are: (*i*) the drastically shortened helix A; (*ii*) the severe alteration of the C-E region; (*iii*) the presence of a long polypeptide segment (pre-F) in extended conformation, and (*iv*) a variable-length helix F that effectively supports the proximal HisF8 residue coordinated to the heme Fe atom (Pesce et al., 2013).

A distinct aspect of groups I and II is the presence of cavities inside the structure linking the protein surface to the distal heme, responsible for storage and diffusion of ligands to/from the heme. The 2/2Hbs generally display moderate to very low O_2-dissociation rates, and thus moderate to high O_2 affinity, due to the presence of at least one hydrogen-bond between the heme Fe-bound ligand and the protein matrix, most commonly provided by TyrB10, TrpG8, His or Tyr at CD1 and GlnE11 (Pesce et al., 2013; Bustamante et al., 2016).

The genome of the cold-adapted bacterium *Pseudoalteromonas haloplanktis* TAC125 (*Ph*TAC125) contains multiple genes encoding three distinct 2/2Hbs (Giordano et al., 2007), supporting the hypothesis of their involvement in several functions, including protection against oxidative and nitrosative stress in the cold and O_2-rich environment of Antarctica. In particular, *Ph*TAC125 also hosts one 2/2HbI (encoded by the *PSHAa0458* gene), two distinct 2/2Hbs of group II (*Ph*-2/2HbO-0030 and *Ph*-2/2HbO-2217, encoded by the *PSHAa0030* and *PSHAa2217* genes, respectively), and one FHb, annotated as PSHAa2880 (Giordano et al., 2007). It is worth noting that

Ph-2/2HbO-0030 and *Ph*-2/2HbO-2217 are both endowed with hexa-coordination (Giordano et al., 2011; Howes et al., 2011; Russo et al., 2013; Giordano et al., 2015; this study).

Ph-2/2HbO-0030 has been extensively characterised by spectroscopic analysis, kinetic measurements, computer simulation and X-ray crystallography by some of the present authors (Howes et al., 2011; Giordano et al., 2011, 2013, 2015; Russo et al., 2013). The results indicate unique adaptive structural properties that enhance the overall flexibility of the protein (Giordano et al., 2015). Recent results on a genomic mutant strain highlight the involvement of cold-adapted *Ph*-2/2HbO-0030 in protection against stresses induced by high O_2 concentration (Parrilli et al., 2010) and RNS (Coppola et al., 2013).

In the genome of *Ph*TAC125, two 2/2 globins *Ph*-2/2HbO-0030 and *Ph*-2/2HbO-2217 encoding genes are constitutively transcribed, thus suggesting that these 2/2Hbs are not functionally redundant in their physiological function in *Ph*TAC125. Thus, the putative role of the *Ph*-2/2HbO-2217 globin was investigated in the present study by integrating *in vivo* and *in vitro* results, with the aim of shedding light on its physiological role, with special attention to involvement in the RNS detoxification mechanisms, in the context of analyzing specific functional hypotheses.

The *PSHAa2217* gene was cloned and over-expressed in the FHb-deficient mutant of *Escherichia coli* and the growth properties and O_2 uptake in the presence of NO of the mutant carrying the *PSHAa2217* gene were analysed. The ferric form of *Ph*-2/2HbO-2217 is able to catalyse peroxynitrite isomerisation *in vitro*, indicating its potential role in the scavenging of RNS. Here we present *in vitro* evidence for the detoxification of NO by *Ph*-2/2HbO-2217.

2. Materials and Methods

2.1. Sequence alignment

Sequence alignment was performed by the program CLUSTAL OMEGA and manual adjustments were based on known crystal structures. The 2/2Hbs belonging to Group II are: *Ph*-

2/2HbO-2217, *Ph*-2/2HbO-0030 (Giordano et al., 2015), *Thermobifida fusca* (*Tf*-2/2HbO) (Bonamore et al., 2005), *Mycobacterium tuberculosis* (*Mt*-2/2HbO) (Milani et al., 2003), *M. leprae* (*Ml*-2/2HbO) (Visca et al., 2002), *Agrobacterium tumefaciens* (*At*-2/2HbO) (Pesce et al., 2011), *Bacillus subtilis* (*Bs*-2/2HbO) (Giangiacomo et al., 2005), and *Geobacillus stearothermophilus* (*Gs*-2/2HbO) (Ilari et al., 2007). The homology model of *Ph*-2/2HbO-2217, using the 3D-structure (PDB ID 4UUR) of *Ph*-2/2HbO-0030 as template, was built with SwissModel (https://swissmodel.expasy.org/) (Arnold et al., 2006, 2011; Biasini et al., 2014).

2.2. Strains and culture conditions

Since the FHb (Hmp) from *E. coli* provides a highly effective detoxification mechanism for NO, we used strain RKP3036 (carrying a genomic *hmp* null mutation) for cloning and expressing the *PSHAa2217* gene, to test cell survival and O_2 uptake in the presence of nitrosative stress. *E. coli* RKP3919 (*E. coli* RKP3036 carrying the empty vector pBAD/HisA) was used as a negative control. *E. coli* RKP3910 strain [*E. coli* RKP3036 transformed with the pPL341 vector carrying the wild-type *hmp*$^+$ gene (Vasudevan et al., 1991)] and *E. coli* RKP3036 carrying the *PSHAa0030* gene (Coppola et al., 2013) were used as positive controls. The *E. coli* TOP10 strain was used for cloning and expressing the *PSHAa2217* gene, and to purify the protein *Ph*-2/2HbO-2217. Cells were grown in Luria-Bertani (LB) medium, pH 7.0, at 25 °C, 180 rpm and under aerobic conditions. When required, ampicillin (Amp, 100 µg/mL) and kanamycin (Km, 35 µg/mL) were added.

2.3. Cloning and expression of the PSHAa2217 gene

The primer pairs forward (5′-TATGAGTGAGCCATGGATACTAAAGT-3′) and reverse (5′-GCGGGATCCCTAGCTACCCGATACCATTCT-3′) were designed on the basis of the *PSHAa2217* gene sequence encoding *Ph*-2/2HbO-2217 (Médigue et al., 2005). The sequence corresponding to the *Nco*I site was introduced in the forward primer. The *PSHAa2217* gene was retrieved from the genomic DNA of *Ph*TAC125 using the PCR approach. The amplified fragment

153 was directly cloned into the pTZ57R/T vector and sequenced to verify its authenticity.

154 The *Nco*I-*Pst*I digested fragment of the *PSHAa2217* gene was further cloned into the
155 corresponding sites of the L-arabinose-inducible, Amp-resistant, and His-tagged pBAD/HisA vector
156 (Invitrogen, Carlsbad, CA, USA). The restriction enzyme cut-sites (*Nco*I and *Pst*I) were designed
157 for the insertion of the *PSHAa2217* gene in pBAD/HisA without the His-tagged region. The
158 construction was verified by sequencing and named pBAD-2/2HbO-2217.

159 For over-expression of the globin gene in the *E. coli hmp* mutant and in *E. coli* TOP10, the
160 cells were transformed with plasmid construct pBAD-2/2HbO-2217 and inoculated into LB
161 medium supplemented with Amp (100 μg/mL). For growth of the *E. coli hmp* mutant, Km (35
162 μg/mL) was also added to the medium. Cells were allowed to grow at 25 °C until A_{600} reached ~ 1
163 OD and then supplemented with 0.2 mM δ-aminolevulinic acid, 0.012 mM $FeCl_3$, and 0.06% L-
164 arabinose, and further incubated for 5 h at 25 °C. Expression of the globin was monitored by
165 running the cell lysate of recombinant strains on 15% SDS-PAGE followed by Coomassie Brilliant
166 Blue staining.

167

168 *2.4. Protein purification*

169 Purification of *Ph*-2/2HbO-2217 was achieved by FPLC (GE Healthcare Biosciences,
170 Amersham Biosciences Ltd, UK) anion-exchange chromatography, loading the cell lysate obtained
171 from *E. coli* TOP10 expressing the *PSHAa2217* gene on a Q Sepharose column (HiTrap™ QFF, GE
172 Healthcare Biosciences, Amersham Biosciences Ltd, UK), equilibrated with 20 mM Tris-HCl pH
173 8.2. *Ph*-2/2HbO-2217 was eluted with a NaCl gradient from 0 to 1.0 M. The eluate was further
174 purified by a second anion-exchange chromatography step on a Mono Q-Tricorn column,
175 equilibrated with 20 mM Tris-HCl pH 8.2. The protein was eluted with a NaCl gradient from 0 to
176 250 mM. All buffers were prepared in MilliQ water. The protein obtained was > 98% pure on SDS-
177 PAGE. The *N*-terminal sequence was determined by automatic sequencing performed with an
178 Applied Biosystems Procise 494 automatic sequencer, equipped with on-line detection of

phenylthiohydantoin amino acids.

2.5. Samples for spectroscopic analysis

Ferric *Ph*-2/2HbO-2217 at pH 6.0, 7.6 and 9.9 was prepared in 50 mM MES [2-(*N*-morpholino) ethanesulfonic acid], 20 mM Tris-HCl and 50 mM glycine, respectively. The hydroxyl complex in isotopically enriched water was prepared by washing *Ph*-2/2HbO-2217 in 20 mM Tris-HCl pH 7.6 with 0.1 mM glycine pD 10.2 prepared with D_2O (99.8%) (Merck AG Darmstadt, Germany). Ferrous samples at pH 7.6 were prepared by addition of a freshly prepared sodium dithionite solution (10 mg/mL) to the ferric forms previously flushed with nitrogen. The Fe(II)-CO complex at pH 7.6 was prepared by flushing ferric *Ph*-2/2HbO-2217 firstly with nitrogen, then with ^{12}CO or ^{13}CO (Rivoira, Milan, Italy), and reducing the heme by addition of a freshly prepared sodium dithionite solution (10 mg/mL). All chemicals were of analytical or reagent grade and were used without further purification.

Protein concentration in the range 10–30 μM was used for electronic absorption and Resonance Raman (RR) spectroscopies at both room and low temperature. The concentration used for Electron Paramagnetic Resonance (EPR) spectroscopy was 100 μM. The protein concentration was estimated on the basis of the molar absorptivity of the ferric form at 408 nm, $\varepsilon = 131\ mM^{-1}\ cm^{-1}$.

2.6. Electronic absorption measurements

UV-visible absorption spectra of whole cells of *E. coli hmp* carrying pBAD/HisA and pBAD-2/2HbO-2217 were recorded using an SDB-4 dual-wavelength scanning spectrophotometer (University of Pennsylvania Biomedical Instrumentation Group, and Current Designs, Inc., Philadelphia, PA) at room temperature (Kalnenieks et al., 1998). Samples were generally scanned with a 0.5-nm step size. Data were analysed using SoftSDB (Current Designs) and Sigma Plot 11.0 (Systat Software, Inc., San Jose, CA, USA).

205 Aerobic cultures were grown overnight (for about 18 h) in flasks containing medium up to 1/5
206 of their volume with appropriate antibiotics and supplements in different concentrations. Cells were
207 harvested by spinning at 5500 rpm for 15 min at 4 °C and the pellets were re-suspended in 6 mL of
208 0.1 M sodium phosphate buffer, pH 7.0. Spectra were recorded between 400 nm and 700 nm. All
209 spectra were baseline-corrected.
210 UV-visible absorption spectra of cell lysates of *E. coli hmp* carrying either pBAD/HisA or
211 pBAD-2/2HbO-2217 were measured with a double-beam Cary 300 spectrophotometer (Agilent
212 Technologies, Santa Clara, CA, USA), using a 120-nm/min scan rate. Pellets, prepared as already
213 described, were re-suspended in 50 mM Tris-HCl buffer pH 7.4, containing 2 mM $MgCl_2$ and 1
214 mM EGTA; cells were disrupted by sonication. The debris was pelleted by centrifugation at
215 12,000×g for 15 min and membranes recovered from the supernatant by ultracentrifugation for 1 h
216 at 225,000×g, 4 °C. The absorption spectra of the supernatants were recorded between 400 and 700
217 nm.
218
219 *2.7. Resonance Raman measurements*
220 The RR spectra were obtained at 25 °C using a 5-mm NMR tube by excitation with the
221 406.7 and 413.1 nm lines of a Kr^+ laser (Innova 300 C, Coherent, Santa Clara, CA, USA), the 514.5
222 nm line of an Ar^+ laser (Innova 90/5, Coherent), and the 441.6 nm line of a He–Cd laser (Kimmon
223 IK4121R-G). Back-scattered light from a slowly rotating NMR tube was collected and focused into
224 a triple spectrometer with spectral resolution as reported elsewhere (Ciaccio et al., 2017). A
225 cylindrical lens, which focuses the laser beam in the sample to a narrow strip rather than the usual
226 point, was used to collect the spectra of both the Fe(II)-CO complex and the ferric sample at pH 7.6
227 in order to avoid photolysis and minimize sample degradation induced by irradiation.
228 The RR spectra were calibrated with indene, *n*-pentane and carbon tetrachloride as standards
229 to an accuracy of 1 cm^{-1} for intense isolated bands. All RR measurements were repeated several
230 times under the same conditions to ensure reproducibility. To improve the signal-to-noise ratio, a

number of spectra were accumulated and summed only if no spectral differences were noted. All spectra were baseline-corrected.

For the low temperature experiments, a 1.5-cm diameter quartz crucible positioned in a THMS600 cryostat (Linkam Scientific Instruments, Surrey, UK) containing ~ 100 µL frozen samples at 80 K was used.

Absorption spectra recorded using a 5-mm NMR tube (300 nm/min scan rate) or a 1-cm cuvette (600 nm/min scan rate) at 25 °C by means of a Cary 60 spectrophotometer (Agilent Technologies, Glostrup, Denmark) (resolution of 1.5 nm), were measured both prior to and after RR measurements to ensure that no degradation occurred under the experimental conditions used. ~~All spectra were baseline-corrected.~~

For the low temperature experiments, a 1.5-cm diameter quartz crucible positioned in a THMS600 cryostat (Linkam Scientific Instruments, Surrey, UK) containing ~ 100 µL frozen samples at 80 K was used.

2.8. EPR measurements

EPR spectra were recorded with an Elexsys E500 (Bruker, Rheinstetten, Germany), equipped with an NMR gaussmeter and a microwave frequency counter. An ESR 900 cryostat (Oxford Instruments, Abingdon, UK), was used to obtain low temperatures. Spectra were recorded under non-saturating conditions at 5 K, 1-mW microwave power and 1-mT modulation amplitude. The *g* values were determined by careful visual inspection of the spectra.

2.9. *S-nitrosoglutathione and NO-donors*

Three different agents of nitrosative stress were used, according to the experimental design. For growth experiments, a source of NO gas was compared with a nitrosating agent. As a source of NO, DETA-NONOate (Enzo Life Science, Farmingdale, NY, USA) with a half-life of 20 h at 37 °C and 56 h at 22–25 °C in 0.1 M phosphate buffer pH 7.4 was used; thus NO release and provision to

257 the bacteria were prolonged over several hours. The nitrosating agent *S*-nitrosoglutathione (GSNO)
258 was prepared as previously reported (Hart, 1985). It is widely used in microbial growth experiments
259 because it is moderately stable in aqueous solutions; however, a derived nitrosated dipeptide, S-
260 nitroso-L-cysteinylglycine, is transported inwards (via the Dpp-encoded dipeptide permease in
261 certain bacteria) and intracellular transnitrosation reactions ensue (Laver et al., 2012). In contrast, for
262 short-term respiration experiments designed to test the addition of a bolus of NO, we used Proli-
263 NONOate (Bioquote Limited, York, UK) with a half-life of 1.8 s at 37 °C in 0.1 M phosphate buffer
264 pH 7.4. All experiments were performed in triplicate.
265
266 *2.10. GSNO and NO susceptibility*
267 Cultures of the *E. coli hmp* mutant, transformed with pBAD/HisA (negative control), pBAD-
268 2/2HbO-0030 (positive control) (Coppola et al., 2013) and pBAD-2/2HbO-2217, were grown in
269 plastic universal tubes in 2 mL of LB medium containing appropriate antibiotics and incubated for
270 2.5 h at 25 °C. The culture was then supplemented with: 0.2 mM δ-aminolevulinic acid, 0.012 mM
271 $FeCl_3$, L-arabinose at the final concentration of 0.06% for *E. coli hmp* carrying either *Ph*-2/2HbO-
272 2217 or the empty vector, and at the final concentration of 0.2% for the positive control *E. coli hmp*
273 carrying *Ph*-2/2HbO-0030 (as in Coppola et al., 2013). GSNO and DETA-NONOate were later
274 added to all tubes at different concentrations (GSNO: 0, 1, 3, and 5 mM; DETA-NONOate: 0, 0.5, 1,
275 and 2 mM).
276 The cultures were incubated for approximately 18 h in the dark, at 25 °C with shaking, and
277 then the optical density at 600 nm was recorded.
278
279 *2.11. Growth curves*
280 Cultures of the *E. coli hmp* carrying different plasmids were grown in the dark in 250 mL
281 flasks containing 10 mL of medium with appropriate antibiotics. Induction supplements (for details

see section on GSNO and NO susceptibility), GSNO (3 mM) or DETA-NONOate (0.5 mM) were added to each flask, at t = 2.5 h.

2.12. NO uptake and cellular respiration

Cultures of the *E. coli hmp* mutant carrying pBAD-2/2HbO-2217, pBAD-2/2HbO-0030, and pBAD/HisA were grown in 250 mL flasks containing 40 mL of LB medium, supplemented with the appropriate antibiotics. Induction supplements were added when the cells reached an OD of 1.0. Cultures were grown overnight (around 18 h), at 25 °C. Cells were harvested at 5500 rpm for 15 min at 4 °C; the pellets obtained were washed twice with 10 mL 50 mM Tris-HCl buffer pH 7.5, then re-suspended in 5-10 mL of the same buffer to normalise the optical density (OD) of the suspensions.

The respiration rates of whole cells were measured using a Clark-type polarographic O_2 electrode (Rank Bros, Bottisham, Cambridge, UK) operating at a polarising voltage of 0.60 V. The apparatus consists of a Perspex chamber kept at 25 °C using a water jacket around the chamber and stirred magnetically with a membrane-covered electrode placed at the bottom of the chamber (Stevanin et al., 2000). The electrode was calibrated using air-saturated buffer, which was then treated with a small amount of sodium dithionite to achieve anoxia. Parallel measurements of O_2 and NO were made by housing a World Precision Instruments (Sarasota, FL, USA) ISO NOP sensor (2-mm diameter) in the same vessel (Mills et al., 2001); note that the ingress of air around the NO port results in slow backflow of O_2 into the chamber contents.

The NO electrode was calibrated as described by the manufacturer (World Precision Instruments, Sarasota, FL, USA). Briefly, sequential volumes of 50 μM $NaNO_2$ (e.g. 100, 200, 400, and 800 μL) were added under stirring to 20 mL of 0.1 M H_2SO_4/KI, in which the NO electrode was suspended.

After calibration of the O_2 and NO electrodes, the whole cell suspension was diluted with 50 mM Tris-HCl pH 7.5 in the O_2-electrode chamber to a final volume of 2 mL, and closed with a tight-fitting lid . The respiration was started using 25 mM glucose. Proli-NONOate (final

concentration, 1 μM) was added through a hole in the vessel lid using a Hamilton syringe, at progressively lower O_2 concentrations. Respiration was followed until the chamber became devoid of O_2.

2.13. Heme assay

Absorption spectra of sonicated samples (0.6 mL without clarification) containing 0.6 mL of reagent (0.4 M NaOH, 4.2 M pyridine) were taken in a quartz cuvette (with stopper) and analysed between 500 and 700 nm using a double-beam Cary 300 spectrophotometer with a 120-nm/min scan rate. Each sample was reduced by adding small amounts of sodium dithionite followed by gentle stirring. A sample was used to obtain the oxidised spectrum by addition of potassium ferricyanide. Difference spectra of reduced *vs* oxidised forms were obtained; the heme concentration was calculated from the absorbance difference at 556 and 539 nm for the dithionite-reduced and ferricyanide-oxidised samples, respectively.

2.14. Peroxynitrite isomerisation

Peroxynitrite was obtained from Cayman Chemical Company (Ann Arbor, MI, USA). The concentration of peroxynitrite was determined spectrophotometrically by measuring the absorbance at 302 nm ($\varepsilon = 1.705\times10^3$ M^{-1} cm^{-1}). The peroxynitrite stock solution (2.0×10^{-3} M) was diluted immediately before use with degassed 1.0×10^{-2} M NaOH to reach the desired concentration (Bohle et al., 1996; Koppenol et al., 1996; Herold and Shivashankar, 2003; Herold et al., 2004a; Ascenzi and Fasano, 2007; Goldstein and Merényi, 2008).

Kinetics of peroxynitrite isomerization, by ferric *Ph*-2/2HbO-2217 and *Ph*-2/2HbO-0030, in the absence and presence of cyanide (final concentration, 5.0×10^{-4} M), was recorded at 302 nm ($\varepsilon = 1.705\times10^3$ M^{-1} cm^{-1}) by rapidly mixing the buffer solution (1.0×10^{-1} M bis-tris-propane buffer, pH 7.4) or the ferric globin solutions (final concentration, 4 to 16 μM; 1.0×10^{-1} M bis-tris-propane buffer, pH 7.4) with the peroxynitrite solution (final concentration, 2.5×10^{-4} M).

In the absence and presence of ferric globins and cyanide, values of the pseudo-first-order rate constant for peroxynitrite isomerization (i.e. k) were determined from the analysis of the time-dependent absorbance decrease at 302 nm, according to Eq. (1):

$$[\text{peroxynitrite}]_t = [\text{peroxynitrite}]_t \times e^{-k \times t} \quad (1)$$

Values of the second-order rate constant for peroxynitrite isomerization by ferric *Ph*-2/2HbO-2217 and *Ph*-2/2HbO-0030 (*i.e.*, k_{on}) and of the first-order rate constant for the spontaneous conversion of peroxynitrite to nitrate (i.e. k_0) were determined from the dependence of k_{on} on the ferric globin concentration, according to Eq. (2):

$$k = k_{on} \times [Ph\text{-}2/2HbO\text{-}2217\text{-}Fe(III)] + k_0 \quad (2)$$

3. Results

3.1. Primary structure

Figure 1A shows the alignment of *Ph*-2/2HbO-2217 and *Ph*-2/2HbO-0030 with some representative 2/2Hbs belonging to group II. The sequence identity between the two Antarctic globins is only 24%, thus suggesting that these proteins may play different function(s) in bacterial physiology.

The main difference between *Ph*-2/2HbO-2217 and *Ph*-2/2HbO-0030 is the presence in the former of a longer sequence extension at the *N* terminus (19 residues in *Ph*-2/2HbO-0030 and 9 residues in *Ph*-2/2HbO-2217), rarely observed in 2/2Hbs. In *Ph*-2/2HbO-0030, the extension is proteolytically cleaved during protein purification (Giordano et al., 2007), and it does not appear to be a requirement for NO detoxification (Coppola et al., 2013).

By comparison with other group II globins , and taking *Mt*-2/2HbO as the reference, the two Antarctic globins show: (i) a three-residue insertion in the BC loop, (ii) one-residue deletion in the CE loop, (iii) three-residue deletion in the GH loop and at the *C* terminus (Giordano et al., 2015, this study), (iv) His and Trp residues at positions F8 and G8, respectively, (v) the Phe-Tyr motif at

positions B9-B10, and (vi) a His residue at position CD1. The analysis of all bacterial sequences available to date (~ 1100) demonstrated that the CD1 position is occupied predominantly by Phe and in some cases by His or Tyr (~ 20 and 15%, respectively) (Bustamante et al., 2016). His (a hydrogen bonding residue) at the topological position CD1 site is always matched by a hydrophobic E11 residue (Leu or Phe). Thus, one of the necessary hydrogen bonding elements involved in ligand stabilisation is alternatively located at opposite edges of the heme distal cavity, either at the CD1 or at the E11 sites, but never simultaneously. In *Ph*-2/2HbO-2217, the E11 residue is Leu, while it is Phe in *Ph*-2/2HbO-0030.

In *Ph*-2/2HbO-0030 the two Gly-Gly motifs, located in the AB and EF hinges of 2/2Hbs belonging to groups I and II, are present and help to stabilize the short helix A in a conformation locked onto helices B and E. In contrast, in *Ph*-2/2HbO-2217 the second Gly residue is replaced by Glu at the AB hinge.

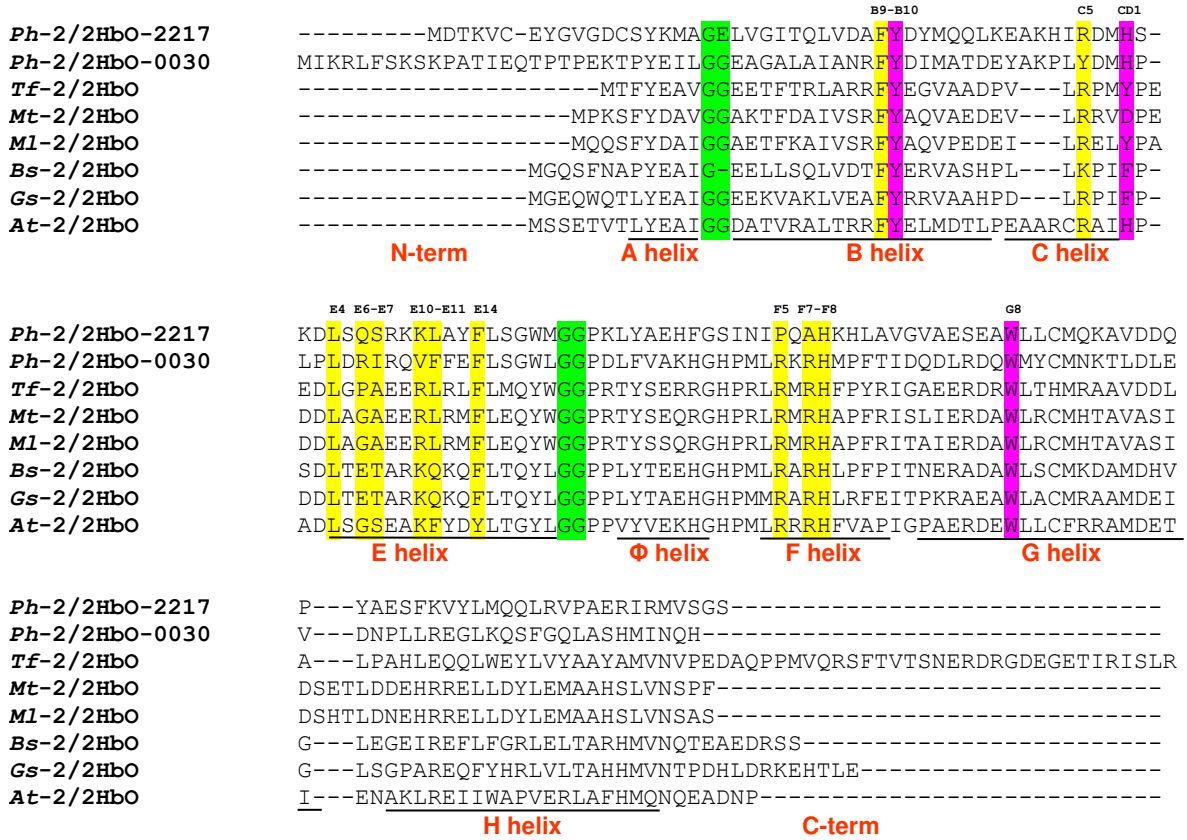

Figure 1A. Sequence alignment, carried out by Clustal Omega, of *Ph*-2/2HbO-2217 and *Ph*-2/2HbO-0030 compared with other members of group-II. Manual adjustments have been based on known crystal structures adapted from Giordano et al. (2015). Functionally important residues are shown in yellow; residues (B10, CD1 and G8) specific for 2/2Hbs of group-II are in purple; the Gly-Gly motifs are in green. Helical regions (A-H) are indicated by black bars and helix Φ, specific for 2/2Hb of group-II, is shown. The numbering of residues is based on the position of residues in the helices of sperm whale Mb, adapted from Giordano et al. (2015).

Position E7 is variable in group II globins and is usually occupied by a small residue (typically Ala, Ser or Thr), thus suggesting an E7 route entry path to facilitate the accessibility of diatomic ligands to the heme distal site (Milani et al., 2003; Vuletich and Lecomte, 2006; Nardini et al., 2007; Pesce et al., 2013). In *Ph*-2/2HbO-2217, E7 is occupied by Ser (**Figure 1B**), whereas in *Ph*-2/2HbO-0030 by Ile, separating the heme distal cavity from the solvent region (Giordano et al., 2015).

Figure 1B overlays the heme pocket of a *Ph*-2/2HbO-2217 homology model and the *Ph*-2/2HbO-0030 structure used as template, showing different residues involved in the stabilisation of the heme through Fe coordination. In *Ph*-2/2HbO-0030, the heme was found to be stabilized through direct Fe coordination to proximal His(96)F8, electrostatic interactions with the heme propionates, and van der Waals contacts (< 4.0 A) with 23 residues. In particular, propionate D is stabilized by an H-bonded salt bridge with Arg(95)F7, and propionate A is electrostatically coupled to Arg64; in addition, both propionates are H-bonded with a water molecule (Giordano et al., 2015). However, in *Ph*-2/2HbO-2217 the propionate-protein interactions are quite different. In *Ph*-2/2HbO-2217, position EF6 is occupied by Tyr (**Figure 1B**), highly conserved in 2/2Hbs of group II (Bustamante et al., 2016), but not present in *Ph*-2/2HbO-0030 (Phe was found instead) (Giordano et al., 2015). Therefore, the formation of an additional H bond with propionate D is predicted. However, Arg at F7, present in other 2/2Hbs and conserved in *Ph*-2/2HbO-0030, is replaced by Ala in *Ph*-2/2HbO-2217. Moreover, Arg(64)E6, electrostatically coupled to propionate A in *Ph*-2/2HbO-0030

(Giordano et al., 2015), in *Ph*-2/2HbO-2217 is replaced by Gln.

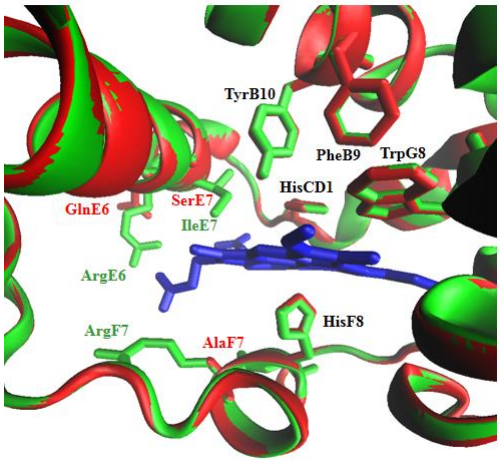

Figure 1B. Superimposition of the heme pocket of a *Ph*-2/2HbO-2217 homology model (red) and the *Ph*-2/2HbO-0030 template structure (green). The heme group is in blue. The residues involved in the stabilisation of the heme through Fe coordination are shown (B9, B10, CD1, G8, E6, E7, F7, F8), as reported in Giordano et al. (2015).

3.2. Spectroscopic characterisation

3.2.1. Ferric Form

Figure 2 compares the UV-vis and the RR high-frequency region (at 298 and 80K) spectra of ferric *Ph*-2/2HbO-2217 at different pH. At pH 6.0, room-temperature spectra (**panels A, B)** are characteristic of a predominantly hexa-coordinate (6c) high-spin (HS) (aquo) form [charge-transfer (CT1) band at 632 nm and RR bands at 1483 (ν_3), 1558 (ν_2) cm^{-1}]. However, a weak 6c low-spin (LS) form [α band at 577 nm, RR bands at 1509 (ν_3), 1641 (ν_{10}) cm^{-1}], is also present. As in *Ph*-2/2HbO-0030, *Ph*-2/2HbO-2217 undergoes an acid-alkaline transition.

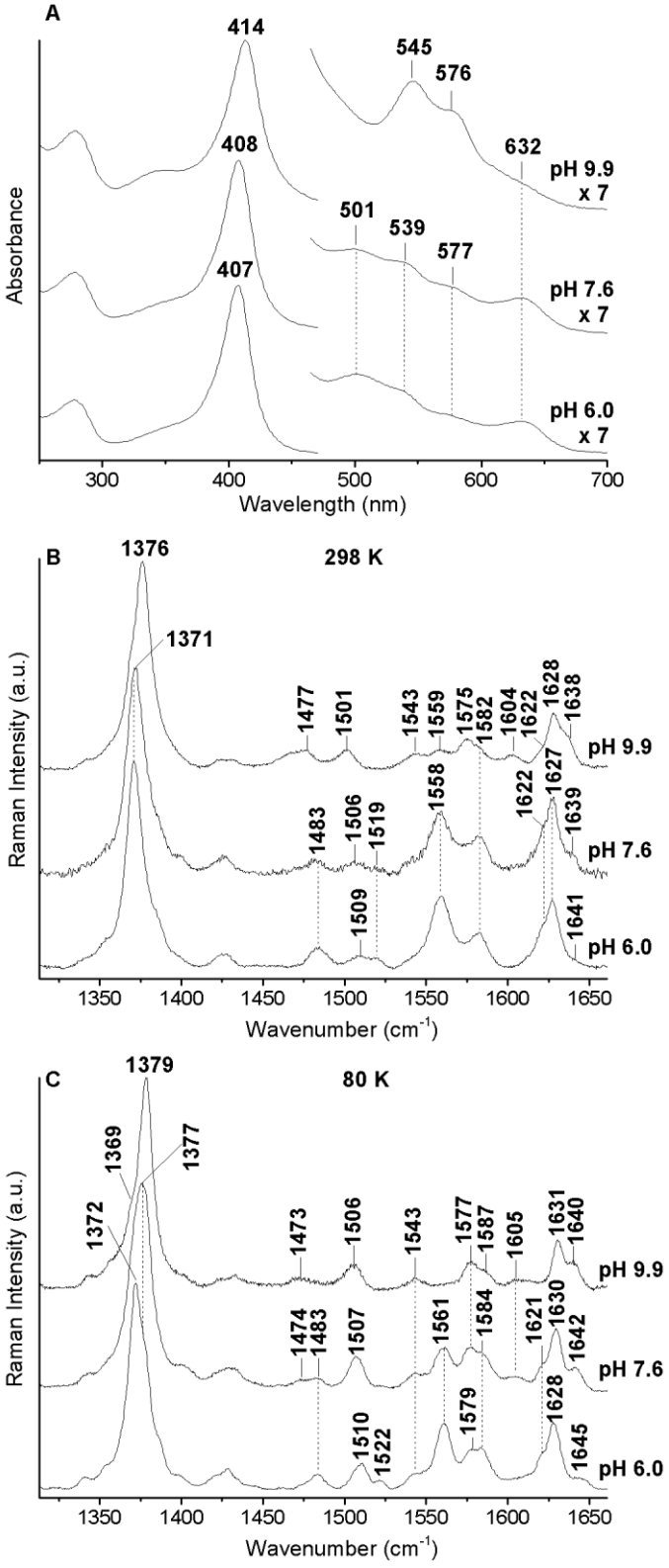

418

419 **Figure 2**. Comparison of the UV-Vis (panel A) and RR spectra in the high frequency region at 298

420 K (panel B) and 80 K (panel C) of ferric *Ph*-2/2HbO-2217 at pH 6.0 (bottom), 7.6 (middle) and 9.9

421 (top). The spectra in all the panels have been shifted along the ordinate axis to allow better

422 visualisation. The 470–700-nm region of the UV-Vis spectra has been expanded 7-fold. RR

experimental conditions: 298 K: excitation wavelength 406.7 nm; (pH 6.0), laser power at the sample 5 mW, average of 4 spectra with 20-min integration time; (pH 7.6), laser power at the sample 4 mW, using a cylindrical lens and cooling the sample with a gentle flow of N_2 passed through liquid N_2, average of 13 spectra with 13-min integration time; (pH 9.9), excitation wavelength 413.1 nm, laser power at the sample 10 mW, average of 3 spectra with 15-min integration time; 80 K: (pH 6.0 and 7.6), excitation wavelength 406.7 nm, laser power at the sample 10 mW, average of 3 spectra with 30-min integration time; (pH 9.9), excitation wavelength 413.1 nm, laser power at the sample 5 mW; average of 12 spectra with 60-min integration time. The intensities of the RR spectra are normalised to that of the ν_4 band.

Hence, upon increasing pH, the 6cHS aquo and 6cLS forms decrease in intensity, and the new OH^--ligated forms, both 6cHS and 6cLS, grow in. At pH 9.9 (one unit lower than for *Ph*-2/2HbO-0030), the UV-Vis and RR spectra are typical of an OH^--ligated form, both 6cHS [1477 (ν_3), 1559 (ν_2) cm^{-1}] and 6cLS [1501(ν_3), 1575 (ν_2), 1638 (ν_{10}) cm^{-1}]; however, unlike for *Ph*-2/2HbO-0030, no 5cHS form is observed. The full assignment of the RR bands, based also on experiments carried out with excitation at 514.5 nm (**Figure S1**), is reported in Table S1.

The spectral dependence on pH is clearly observed in the RR spectra at low temperature (**Figure 2, panel C**). In fact, upon lowering the temperature, the sharpening of the bands and the presence of only a 6cLS OH^- ligated form at alkaline pH facilitate the identification of different 6cLS forms at pH 6.0 and 9.9 characterised by different RR frequencies, which are, on the other hand, both present at intermediate pH 7.6. Accordingly, in addition to a 6cHS form ($g_\perp \sim 6$ and $g_\parallel$ 2.00), the EPR spectrum at pH 7.6 (**Figure S2**) displays two 6cLS forms: one with $g_1 = 2.95$, attributable to His–Fe–Tyr coordination, similar to *Ph*-2/2HbO-0030 (Giordano et al., 2015), and the other with $g_1 = 2.71$, typical of His–Fe–OH^- coordination, absent in *Ph*-2/2HbO-0030 at pH 7.6, but present at pH 10.7 (Giordano et al., 2015).

Figure 3 compares the low-frequency RR spectra of *Ph*-2/2HbO-2217 at alkaline pH in H_2O and D_2O buffered solutions, at 298 K (**panel A, left**) and 80 K (**panel B, left**) together with the difference spectra H_2O - D_2O (**Figure 3, right**).

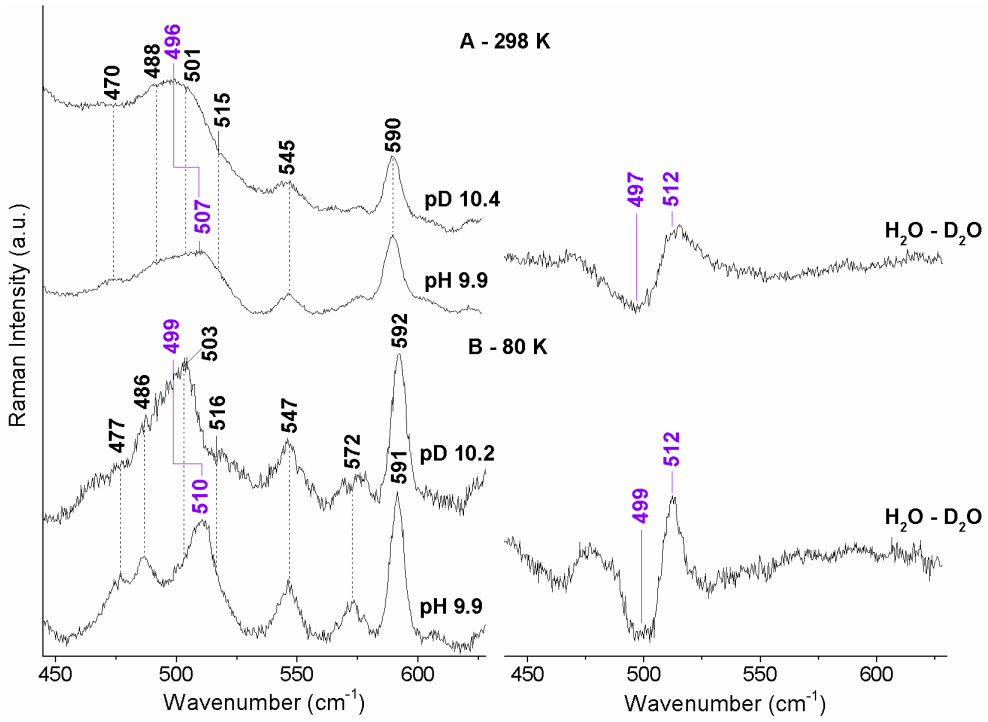

Figure 3. Comparison of the low-frequency region RR spectra at alkaline pH of ferric *Ph*-2/2HbO-2217 at room (panel A, left) and low temperature (panel B, left) in H_2O (bottom) and D_2O (top). The corresponding difference spectra H_2O - D_2O are also shown (panels A and B, right). The ν(Fe-OH) and ν(Fe-OD) mode frequencies are reported in purple. The spectra have been shifted along the ordinate axis to allow better visualisation. The intensity of the spectra is normalised to that of the ν_4 band. Experimental conditions: excitation wavelength 413.1 nm; pH 9.9; laser power at the sample 10 mW, average of 9 spectra with 45-min integration time (298 K) and of 3 spectra with 60-min integration time (80K); pD 10.2: laser power at the sample 10 mW, average of 7 spectra with 70-min integration time (298 K) and laser power at the sample 5 mW, average of 4 spectra with 40-min integration time (80 K).

The 450-530 cm^{-1} region of the spectra is quite complex, due to the porphyrin modes (see **Tables S1 and S2**). However, on the basis of the isotopic substitution, the bands at 507 and 510 cm^{-1} at 298 and 80 K, respectively, which shift to 496 and 499 cm^{-1} in D_2O at 298 and 80 K, respectively, have been assigned to the ν(Fe-OH) mode of a His–Fe–OH^- 6cLS form. Accordingly, the difference spectrum at 80 K shows narrow and well-defined bands at 499 and 512 cm^{-1}. The difference spectrum at 298 K shows two broad bands at 497 and 512 cm^{-1}, possibly due to the concomitant presence of a His–Fe–OH^- 6cHS form observed at room temperature in the RR high-frequency region (**Figure 2, panel B**).The frequency of the *Ph*-2/2HbO-2217 ν(Fe-OH) mode is about 18 and 46 cm^{-1} lower than that observed for *Ph*-2/2HbO-0030 (525 cm^{-1} at 298 K, Giordano et al., 2015) and human Hb (553 cm^{-1} at 298 K, Feis et al., 1994), indicating the presence of strong H-bonds between the OH^- ligand and distal residues. In fact, with an increase of the H-bond strength, a decrease of the force constant of the Fe–OH bond, with concomitant decrease of the ν(Fe–OH) stretching frequency, is expected. However, no upshift of the frequency is observed in D_2O, as in *Ph*-2/2HbO-0030 (543 cm^{-1}, Giordano et al., 2015) or other heme proteins in the presence of strong H-bonds (Nicoletti et al., 2014; Howes et al., 2015). Moreover, due to the instability of *Ph*-2/2HbO-2217 in $H_2{}^{18}O$ buffer, the identification of any ν(Fe–OH) band on the basis of its sensitivity to ^{18}O substitution was not possible.

Therefore, in general, the spectroscopic features of ferric *Ph*-2/2HbO-0030 and *Ph*-2/2HbO-2217 are similar, the main differences being the lower pK_a for the alkaline transition (about one unit) of *Ph*-2/2HbO-2217 compared to *Ph*-2/2HbO-0030, and the absence of a 5cHS form in *Ph*-2/2HbO-2217 at alkaline pH. Accordingly, the low-frequency regions of the RR spectra of the two proteins are also very similar (**Figure S3**). The only notable differences concern the frequency and/or intensity of the vinyl and propionyl bending modes. The $\delta(C_\beta C_a C_b)$ bending modes of the vinyl groups of *Ph*-2/2HbO-2217 give rise to a broad band centered at 415 cm^{-1}, 5 cm^{-1} higher than in *Ph*-2/2HbO-0030. At present, the significance of these variations is not clear, but they possibly suggest

differences in vinyl orientation, in agreement with the 3-cm^{-1} difference of the ν(C=C) stretching modes (Smulevich et al., 1996; Marzocchi and Smulevich, 2003).

The relative intensity of the $\delta(C_\beta C_c C_d)$-propionyl bending modes is markedly different. In particular, the propionyl mode at 381 cm^{-1} is more intense in *Ph*-2/2HbO-2217 than in *Ph*-2/2HbO-0030. This behaviour is observed also in the ferrous carbonylated complex (see below). The frequency and intensity of this mode has been correlated with the hydrogen-bond strength between the heme-propionate and the nearby residues (Cerda-Còlon et al., 1998). As suggested by the different primary structure of the residues surrounding the heme propionyls, the intensity change of one propionyl mode indicates that the H-bonding interactions are different for the two proteins, and in particular much stronger in *Ph*-2/2HbO-2217.

3.2.2. Ferrous Form

Upon reduction, the UV-Vis and RR high-frequency-region spectra of *Ph*-2/2HbO-2217 clearly reveal the presence of a 6cLS form (Soret band at 420 nm and RR bands at 1493 (ν_3), 1577 (ν_2) cm^{-1}) and a 5cHS form (Soret band at 435 nm and RR bands at 1470 (ν_3), 1558 (ν_2) and 1603 (ν_{10}) cm^{-1}), (**Figure 4**), the latter being much more pronounced in *Ph*-2/2HbO-2217 than *Ph*-2/2HbO-0030 (**Figure S4**). The RR low-frequency-region spectrum of *Ph*-2/2HbO-2217 is characterised by a very strong band at 227 cm^{-1}, assigned to the ν(Fe-Im) stretching mode (**Figure 4**). The frequency of this band is 5-cm^{-1} higher than in *Ph*-2/2HbO-0030 (222 cm^{-1}) (Giordano et al., 2011), indicating a stronger proximal Fe-His bond. The frequency is similar to that of other 2/2Hbs (Egawa and Yeh, 2005), consistent with a staggered orientation of the imidazole ring of the proximal His with respect to the four pyrrole nitrogen atoms of the porphyrin ring, revealed by the crystallographic data of *Ph*-2/2HbO-0030 (Giordano et al., 2015), in contrast to the eclipsed orientation observed in human Hb.

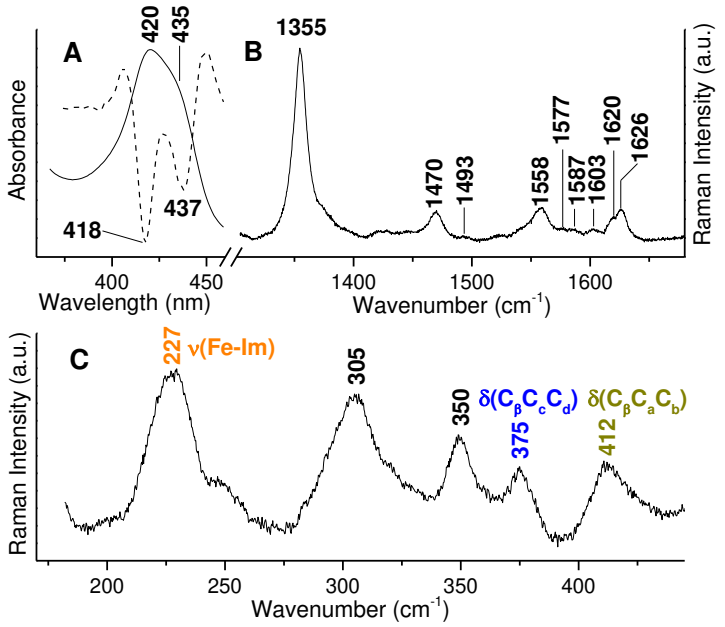

514

515 **Figure 4.** UV-Vis and its the second derivative spectrum (D^2) (dashed line) (panel A), RR spectra in
516 the high- (panel B) and low-frequency region (panel C) of ferrous *Ph*-2/2HbO-2217 at pH 7.6. The
517 spectra have been shifted along the ordinate axis to allow better visualisation. In panel C the ν(Fe-
518 Im), $\delta(C_\beta C_c C_d)$ and $\delta(C_\beta C_a C_b)$ mode frequencies are reported in orange, blue and green,
519 respectively. RR experimental conditions: excitation wavelength 441.6 nm; laser power at the
520 sample 10 mW, average of 4 spectra with 20-min integration time.

521

522 Moreover, similar to the ferric form, slight differences compared to *Ph*-2/2HbO-0030 are
523 evident in the vinyl stretching (1624-1626 cm^{-1}) and bending (409, 412 cm^{-1}) modes.

524 As in *Ph*-2/2HbO-0030 (Giordano et al., 2011), *Ph*-2/2HbO-2217 binds CO, giving rise to a
525 6cLS species. In the RR low-frequency region of the CO adduct (**Figure 5, panel A**), one isotope-
526 sensitive band is identified in both *Ph*-2/2HbO-0030 (494 cm^{-1}) and *Ph*-2/2HbO-2217 (506 cm^{-1}),
527 which shift to 489 and 501 cm^{-1}, respectively, in the case of ^{13}CO (**Figure S5**). These bands are
528 assigned to the ν(Fe–C) stretching mode. Accordingly, a corresponding ν(C–O) stretching mode is
529 observed at 1960 cm^{-1} (*Ph*-2/2HbO-0030) and 1940 cm^{-1} (*Ph*-2/2HbO-2217) (**Figure 5, panel B**),
530 which shift to 1914 cm^{-1} and 1898 cm^{-1}, respectively, upon ^{13}CO substitution (**Figure S5**).

531

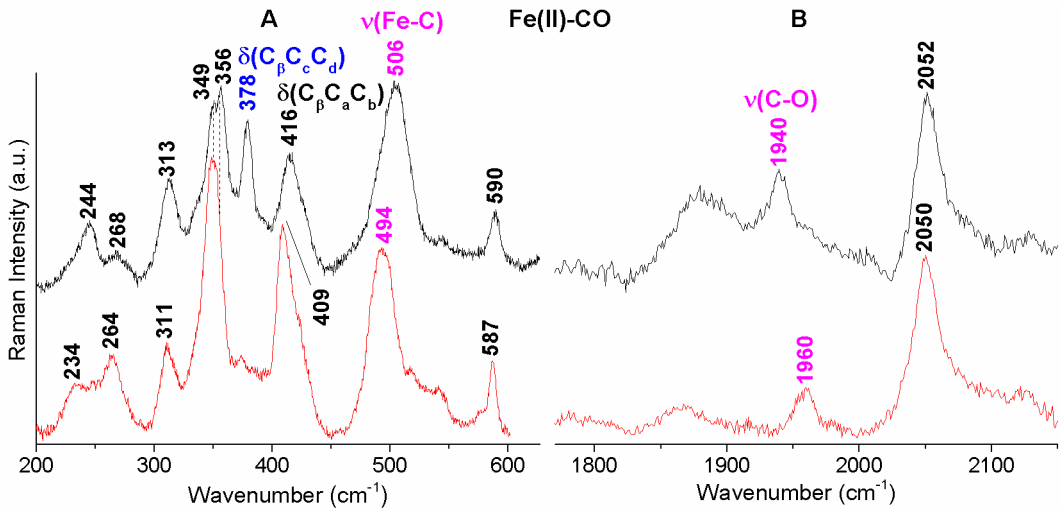

532

533 **Figure 5**. Comparison of the RR spectra of the Fe(II)-^{12}CO complexes of *Ph*-2/2HbO-0030 (red) and
534 *Ph*-2/2HbO-2217 (black) at pH 7.6. The low (panel A) and the high (panel B) frequency regions
535 show the ν(Fe–CO) and ν(C–O) stretching modes (in magenta), respectively. The δ($C_\beta C_c C_d$) mode
536 frequency is shown in blue. The spectra have been shifted along the ordinate axis to allow better
537 visualisation. RR experimental conditions: excitation wavelength 413.1 nm; a cylindrical lens was
538 used to focus the laser beam on the sample; laser power at the sample 2 mW, average of 4 spectra
539 with 10-min integration time (*Ph*-2/2HbO-0030, LF and HF); laser power at the sample 2 mW,
540 average of 3 spectra with 30-min integration time (*Ph*-2/2HbO-2217, LF); average of 9 spectra with
541 90-min integration time (*Ph*-2/2HbO-2217, HF).

542

543 Interestingly, unlike ferrous carbonylated *Ph*-2/2HbO-0030 CO, whose frequencies are
544 characteristic of a CO conformer in which polar interactions with the surrounding residues of the
545 distal cavity are absent, the corresponding CO frequencies for the *Ph*-2/2HbO-2217 CO complex
546 indicate polar interactions between the distal residues and the CO molecule. This finding is
547 consistent also with the presence of strong H-bonds between the OH^- ligand and distal residues, not
548 observed for *Ph*-2/2HbO-0030. Furthermore, the frequency shifts and marked intensity increase of
549 the δ($C_\beta C_c C_d$)-propionate bands upon formation of the CO-complex suggest a change in the
550 environment around the propionate group in *Ph*-2/2HbO-2217 when the hexa-coordinated species is

formed. This is likely consequent to a marked strengthening of the H-bonding interactions between the heme propionates and the nearby residues. Interestingly, in *Ph*-2/2HbO-0030, CO binding causes the complete disappearance of the propionyl bending modes (**Figure 3**), indicating changes in the strength of hydrogen bonding from moderate to weak upon formation of the CO-complex. These observations suggest a flexible heme rocking motion that contributes to the ligand-binding mechanism in the two proteins that might also be influenced by the different H-bonding residues in the vicinity of the propionates for *Ph*-2/2HbO-2217 and *Ph*-2/2HbO-0030.

3.3. Cloning and expression of the PSHAa2217 gene in E. coli *TOP10 cells and in the hmp mutant*

The *PSHAa2217* gene from *Ph*TAC125 was cloned into the commercial vector pBAD/HisA (Invitrogen, Carlsbad, CA, USA), under control of an L-arabinose-inducible promoter. The construct pBAD-2/2HbO-2217 was confirmed by sequencing, and later expressed both in *E. coli* TOP10 cells to purify the protein, and in the *E. coli hmp* mutant to perform *in vivo* function experiments. Since the mutant is very sensitive to NO and RNS, complementation in *trans* of sensitivity indicates that the expressed globin is endowed with detoxification properties. Expression resulted in the accumulation of heme protein inside the cell, giving a reddish brown colour to the recombinant *E. coli* cells. SDS-PAGE demonstrated the presence of a ~15.5-kDa protein corresponding to the expected size of *Ph*-2/2HbO-2217. *Ph*-2/2HbO-2217, cloned and over-expressed in *E. coli* TOP10, was purified by two consecutive anion-exchange chromatography steps (**Figure S6**, **panels A-B**). In agreement with the primary structure of *Ph*-2/2HbO-2217, a ~15.5-kDa protein was obtained (**Figure S6**, **insert C**).

To confirm the expression of the *PSHAa2217* gene in *E. coli hmp*, the UV-visible absorption spectrum of lysate of the cells carrying pBAD-2/2HbO-2217 was compared with that of cells transformed with the empty vector pBAD/HisA (**Figure S7**).

3.4 Growth of the NO-sensitive E. coli *hmp strain carrying Ph-2/2HbO-2217 under nitrosative stress*

The putative role of the globin *Ph*-2/2HbO-2217 was investigated *in vivo* using the *E. coli hmp* mutant to identify NO-detoxification mechanisms. *E. coli hmp* cells carrying *Ph*-2/2HbO-2217 were grown overnight with induction supplements at 25 °C, in the absence and presence of increasing concentrations of either the nitrosating agent GSNO (0, 1, 3, and 5 mM) (**Figure 6A**) or of the NO-releaser DETA-NONOate (0, 0.5, 1, and 2 mM) (**Figure 6B**). The slightly higher concentrations required for GSNO than for DETA-NONOate activity presumably reflect the fact that GSNO releases only low levels of NO (Bowman et al., 2011; Laver et al., 2012) that is detoxified by globins. In fact, 500 µM GSNO releases less NO than 5 µM DEA-NONOate, a relatively fast-releasing NO-donor liberating 1.5 mol per mol parent compound (Jarboe et al., 2008).

The effect of the expression of the *PSHAa2217* gene (**Figure 6**) on the ability of *E. coli hmp* cells to survive in the presence of nitrosative stress was compared to that of cultures of *E. coli hmp* transformed with pBAD/HisA (negative control), or pBAD-2/2HbO-0030 (positive control) (Coppola et al., 2013).

The growth of the *hmp* mutant was progressively inhibited at all GSNO and DETA-NONOate concentrations tested (up to 5 mM GSNO and 2 mM DETA-NONOate). However, exposure to nitrosative stress had no effect on the growth of *E. coli hmp* cells expressing *Ph*-2/2HbO-0030 (Coppola et al., 2013), reflecting complete restoration of NO-detoxifying properties endowed by the FHb. The growth of the *E. coli hmp* mutant carrying the *PSHAa2217* gene was also significantly improved relative to the un-complemented mutant, at 3 mM GSNO (**Figure 6A**) or 0.5 mM DETA-NONOate (**Figure 6B**). These data demonstrate the involvement of both cold-adapted globins in protecting the heterologous host from NO toxicity.

The protein encoded by the *PSHAa2217* gene appeared less efficient in protection from nitrosative stress compared to *Ph*-2/2HbO-0030. However, we cannot exclude the possibility that the lower efficiency of the *Ph*-2/2HbO-2217 compared to *Ph*-2/2HbO-0030 may be due to different levels of expression of these globins. The heme content in the cells carrying the *PSHAa0030* gene was around 2-fold higher than that of *E. coli hmp* carrying the *PSHAa2217* gene.

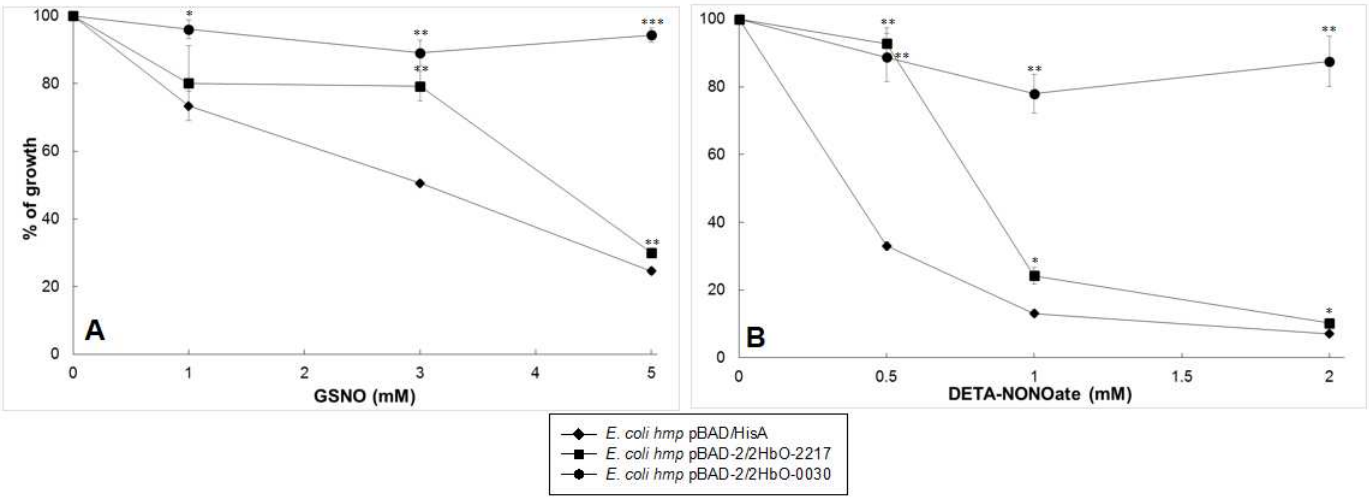

Figure 6. Susceptibility test of *E. coli hmp* expressing different plasmids supplemented with GSNO (A) and DETA-NONOate (B). Cultures of *E. coli hmp* carrying pBAD-2/2HbO-2217 after addition of 0.2 mM δ-aminolevulinic acid, 0.012 mM $FeCl_3$, 0.06% L-arabinose (squares), were grown for 18 h at 25 °C under aerobic conditions, and the optical density was recorded. The same strain, carrying pBAD/HisA (diamonds) and pBAD-2/2HbO-0030 (circles), grown in the presence of 0.2% and 0.06% L-arabinose, respectively, were included as controls. Values are means ± standard deviation. Errors bars of standard deviation were calculated by experiments carried out in triplicate. The significance of the data (*E. coli hmp* expressing *Ph*-2/2HbO-2217 and *Ph*-2/2HbO-0030 compared to *E. coli hmp* with pBAD/HisA) was estimated with a Student's t-test. ***P<0.001; **P<0.01; *P<0.05.

To confirm these results and demonstrate that, similar to *Ph*-2/2HbO-0030, *Ph*-2/2HbO-2217 also confers resistance during growth, cultures of the *E. coli hmp* mutant, carrying pBAD-2/2HbO-2217, pBAD/HisA, or pBAD-2/2HbO-0030, were grown at 25 °C under aerobic conditions and treated with either 3 mM GSNO (**Figure 7A**) or 0.5 mM DETA-NONOate (**Figure 7B**).

In the presence of GSNO, the ability of cells expressing *Ph*-2/2HbO-2217 to grow under nitrosative stress was also compared to that of cultures of *E. coli hmp* transformed with the plasmid

carrying the wild-type *hmp*+ gene from plasmid pPL341 (**Figure 7B**), as an additional positive control (Coppola et al., 2013).

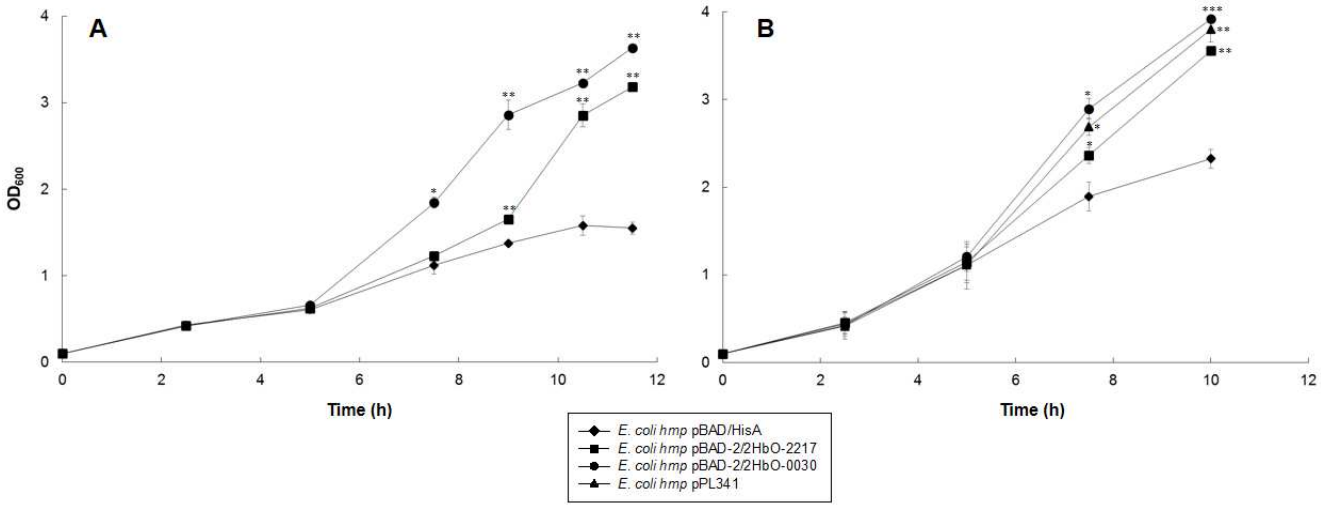

Figure 7. Growth profile of *E. coli hmp* expressing *Ph*-2/2HbO-2217 (squares), *Ph*-2/2HbO-0030 (circles), pBAD/HisA (diamonds), and pPL341 (triangles, Fig. 7B only), exposed to 3.0 mM GSNO (A) and 0.5 mM DETA-NONOate (B). Cultures were grown at 25 °C, under aerobic conditions, and supplemented with 0.2 mM δ-aminolevulinic acid, 0.012 mM $FeCl_3$, L-arabinose at the final concentration of 0.06% for *E. coli hmp* carrying either *Ph*-2/2HbO-2217, the empty vector or pPL341, and at the final concentration of 0.2% for the positive control *E. coli hmp* carrying *Ph*-2/2HbO-0030. Values are means ± standard deviation. Errors bars of standard deviation were calculated by experiments carried out in triplicate. The significance of the data (*E. coli hmp* expressing *Ph*-2/2HbO-2217 and *Ph*-2/2HbO-0030 compared to *E. coli hmp* with pBAD/HisA) was estimated with a Student's t-test. ***P<0.001; **P<0.01; *P<0.05.

Exposure to GSNO caused a slight decrease in growth of the *E. coli hmp* mutant carrying pBAD-2/2HbO-2217 compared to the mutant carrying *Ph*-2/2HbO-0030. In contrast, the growth profile of negative control cells bearing the empty vector pBAD/HisA was drastically reduced. Similar results were obtained in the presence of DETA-NONOate, even if the Antarctic globins

seem to be more effective in protecting growth from inhibition by DETA-NONOate than from GSNO. This may reflect the more complex toxic effects of GSNO (especially nitrosation reactions) (Laver et al., 2012) than NO. It is worth noting that globins detoxify NO but not GSNO *per se* (Laver et al., 2012). In the case of the NONOate, the complete alleviation of growth inhibition by expressing pPL341 encoding the *E. coli* flavohaemglobin Hmp, is clear.

Altogether, these results demonstrate that the globin *Ph*-2/2HbO-2217 provides substantial protection to the cells from NO toxicity in the heterologous host.

3.5. NO consumption and respiration rate of E. coli *hmp expressing the PSHAa2217 gene*

We noted that expression of *Ph*-2/2HbO-2217 was lower in the *hmp* mutant than that of *Ph*-2/2HbO-0030 and so, to eliminate the possibility that this contributed to interpreting measurements of growth and respiration in the presence of nitrosative stress agents, we performed experiments with suspensions of harvested cells in which protein and heme levels were quantified. Cells were grown at 25 °C in the presence of the induction supplements and under aerobic conditions and the respiration of *E. coli hmp* cells carrying the *PSHAa2217* gene, the *PSHAa0030* gene, or the empty vector, exposed to NO toxicity, was measured. Because GSNO is a poor NO donor (Jarboe et al., 2008) and is not a potent inhibitor of cell respiration, the course of O_2 and NO consumption was measured in the presence and absence of the fast NO-releaser Proli-NONOate (**Figure 8**). The toxicity of NO depends on O_2 concentration (Stevanin et al., 2000); thus, additions of NO were made at three different O_2 tensions after stimulating respiration by adding 25 mM glucose. At each NO addition, revealed by a rapid upward excursion of the NO electrode output, the O_2 uptake was abruptly stopped but resumed when the NO levels fell. When NO decreased to a minimal level, respiration continued until the chamber became anaerobic. In the absence of NO, all three strains consumed O_2 at a similar rate when respiration was normalised to total cell protein content, as assessed in the Markwell assay (6.4-8.4 nmol O_2/min/mg) (Markwell et al., 1978). However, when respiration rates were expressed relative to heme content, the strains expressing the globins showed

667 significantly lower respiration rates (6-10 nmol O_2/min/mM heme) than the strain containing the
668 control pBAD/HisA plasmid (15 nmol O_2/min/mM heme); this reflects the lack of globin-catalysed
669 O_2 uptake in the absence of NO.

670 To assess the roles of the two globins in NO detoxification, we measured the rates of O_2 uptake
671 after each NO addition and expressed this relative to the pre-NO rates of O_2 uptake. In Figure 8A,
672 the rate before adding NO (49 nmol O_2/min) was severely reduced by successive NO additions.
673 After each addition there was a transient, almost complete, inhibition of respiration, but activity
674 resumed as the NO concentration declined (as shown by the NO electrode traces). However, the
675 rates never regained the pre-NO rates: in Figure 8A, three successive NO additions resulted in
676 inhibition of >65-73% of the pre-NO rate. In marked contrast, in the case of the two globin-
677 expressing strains (Figure 8B, C), the resumption of O_2 uptake after NO additions regained
678 completely the pre-NO rates and, indeed, an acceleration of O_2 uptake. In the case of *Ph*-2/2HbO-
679 2217, the observed rates were 1.5-2.1-fold higher than the pre-NO rate and in the case of *Ph*-
680 2/2HbO-0030, the observed rates were 1.2-1.7-fold higher than the pre-NO rate.

681 We have already reported the ability of the *E. coli hmp* strain carrying the *PSHAa0030* gene to
682 detoxify NO (Coppola et al., 2013); the present data show that both globins are able to restore
683 respiration to pre-NO rates. We attribute the final stimulation of respiration to the globin-catalysed
684 reaction between the remaining NO and O_2. When O_2 was depleted, further additions of NO resulted
685 in a larger NO signal and in its slower disappearance (**Figure 8A-C**), indicating O_2-dependent NO
686 consumption.

687 Taken together, these results indicate that *Ph*-2/2HbO-2217, like *Ph*-2/2HbO-0030, is able to
688 restore O_2 consumption in vitro after NO challenge, and probably involved in the bacterial defence
689 against nitrosative stress.

690

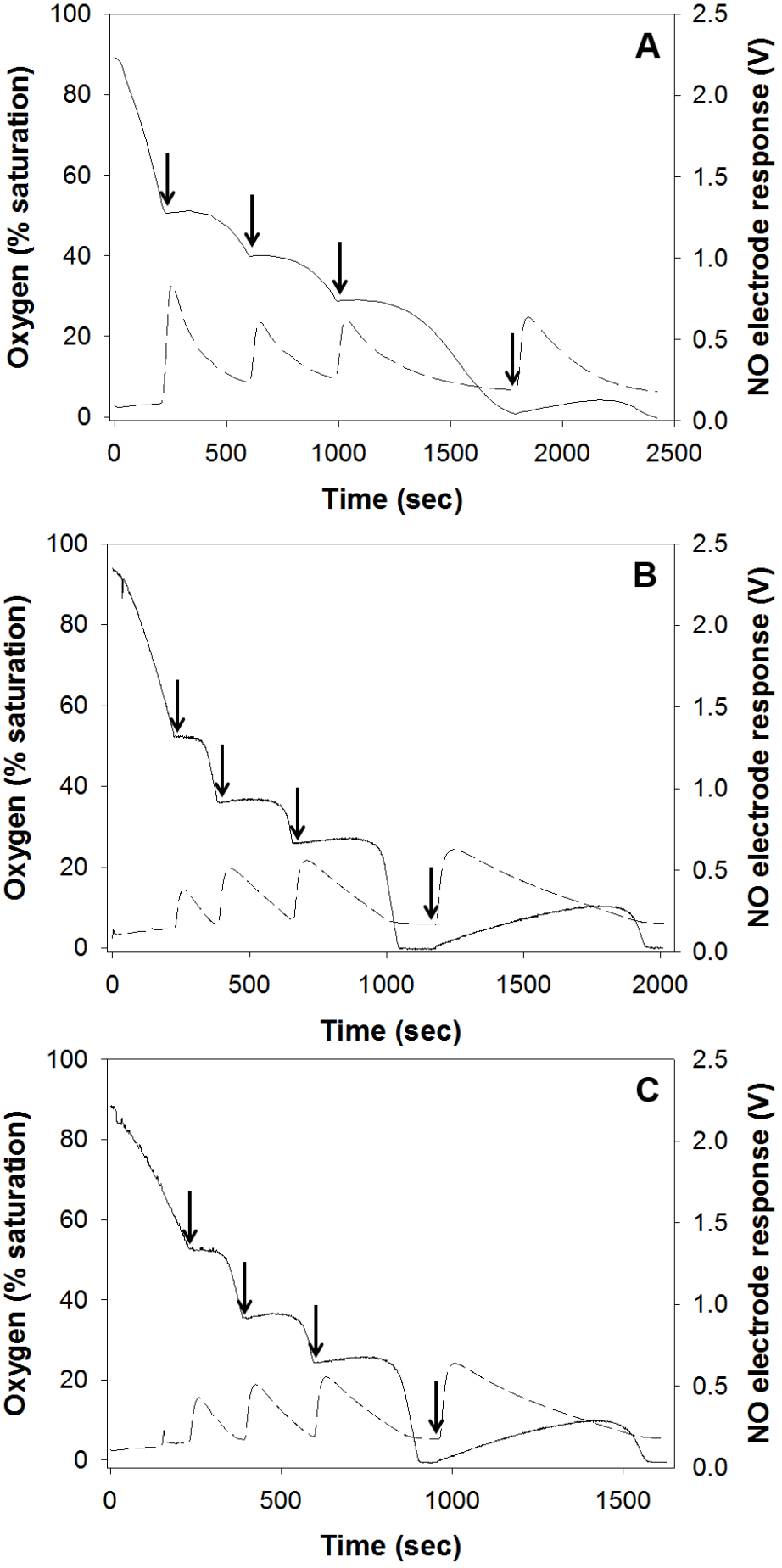
A
B
C
Oxygen (% saturation)
NO electrode response (V)
Time (sec)
0
20
40
60
80
100
0.0
0.5
1.0
1.5
2.0
2.5
0
500
1000
1500
2000
2500

691

692 **Figure 8.** NO uptake and respiration of *E. coli hmp* carrying either the empty vector (pBAD/HisA)
693 (A) or expressing *Ph*-2/2HbO-0030 (B), or *Ph*-2/2HbO-2217 (C). Respiration was followed in a
694 Clark-type O_2 electrode (solid traces) upon additions of 1 μM Proli-NONOate (arrows). NO uptake
695 was measured simultaneously with an NO electrode (dashed traces). After inhibition of respiration
696 by the last aliquot of NO, the slight upward deflections of the O_2 traces probably reflect either the
697 polarographic drift or the back-diffusion of O_2 into the chamber through the Hamilton syringe used
698 to make NO additions. All experiments were performed in triplicate. The volumes of cell
699 suspensions used were adjusted to give similar O_2 uptake rates in the absence of NO.
700
701 *3.6. Peroxynitrite isomerisation*
702 As shown in **Figure 9**, ferric *Ph*-2/2HbO-2217 catalyses peroxynitrite isomerisation, as
703 reported for several globins, e.g. horse heart Mb (Herold and Shivashankar, 2003). On the other
704 hand, cyanide-bound ferric *Ph*-2/2HbO-2217 does not facilitate peroxynitrite isomerisation, as
705 previously reported in hexa-coordinated heme-proteins, e.g. human neuroglobin (Herold et al.,
706 2004b) and horse heart cytochrome *c* (Ascenzi et al., 2011a, b), showing high affinity with
707 intramolecular distal ligands.
708 Under all the experimental conditions, the time course of peroxynitrite conversion to nitrate is
709 a monophasic process for more than 87% of its course. As shown in **Figure 9**, the first-order rate
710 constant k increases linearly with the concentration of ferric *Ph*-2/2HbO-0030 and *Ph*-2/2HbO-
711 2217. The analysis of data shown in **Figure 9** according to Eq. 2 allowed the determination of the
712 k_{on} and k_0 values for peroxynitrite conversion to nitrate by the ferric globins. The values of k_{on}
713 (corresponding to the slope of the linear plot) are 4.0×10^4 M^{-1} s^{-1} and 7.2×10^4 M^{-1} s^{-1} for *Ph*-
714 2/2HbO-2217- and *Ph*-2/2HbO-0030-mediated isomerisation of peroxynitrite, respectively, at pH
715 7.4 and 20 °C.

716 The *y* intercept of the linear plot corresponds to 0.28 s^{-1}, matching with k_0 values (0.30 s^{-1})
717 obtained either in the absence of both ferric globins or in the presence of unreactive ferric globin-
718 cyanide adducts.
719 Interestingly, values of k_{on} for peroxynitrite scavenging by *Ph*-2/2HbO-2217 and *Ph*-2/2HbO-
720 0030 are similar to those reported for sperm whale Mb and human Hb (Herold and Shivashankar,
721 2003), representing the major targets of RNS *in vivo* (Herold and Fago, 2005).
722

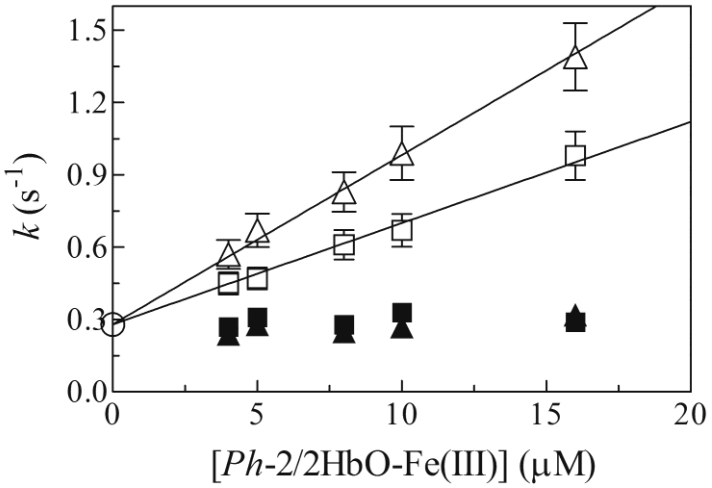

723
724 **Figure 9.** Dependence of *k* for peroxynitrite isomerization on the concentration of ferric *Ph*-
725 2/2HbO-2217, in the absence and presence of cyanide (open and filled squares, respectively). Data
726 for peroxynitrite isomerisation by ferric *Ph*-2/2HbO-0030 in the absence and presence of cyanide
727 (open and filled triangles, respectively) are reported for comparison. All data were obtained at pH
728 7.4 and 20 °C. The circle on the ordinate indicates the value of *k* in the absence of globins. The
729 continuous lines were calculated according to Eq. 2 with $k_{on} = 4.0\times10^4$ M^{-1} s^{-1} (squares) and
730 7.2×10^4 M^{-1} s^{-1} (triangles), and $k_0 = 0.28$ s^{-1}. In the presence of saturating cyanide (5.0×10^{-4} M),
731 values of *k* are independent of the ferric-globin concentration and the average value of k =0.30 s^{-1}
732 corresponds to that of k_0 (circle). The peroxynitrite concentration was 2.5×10^{-5} M. When not
733 shown, the standard deviation is smaller than the symbol. For details, see text.
734

735 **4. Discussion**

736 Life at low temperature imposes a wide array of challenges to marine bacteria. At low
737 temperatures, the enhanced O_2 solubility significantly increases the production rate of ROS.
738 Therefore, bacteria must be able to adjust to temperature changes and availability of nutrients. A
739 genome analysis of *Colwellia psychroerythraea* (Methé et al., 2005) and *Desulfotalea psychrophila*
740 (Rabus et al., 2004) suggests that a common strategy to face environmental challenges consists of
741 developing enhanced antioxidant capacity, resulting from multiple genes that encode catalases and
742 superoxide dismutases.

743 By contrast, in *silico* analysis of the *Ph*TAC125 genome (Médigue et al., 2005) suggests that
744 this Antarctic marine bacterium may cope with increased O_2 solubility by multiplying O_2-
745 scavenging enzymes (such as dioxygenases) and deleting entire metabolic pathways that generate
746 ROS as side products. Moreover, its resistance to H_2O_2 is due to the presence of several enzymes
747 involved in scavenging chemical groups affected by ROS (such as peroxiredoxins and peroxidases),
748 and one catalase-encoding gene (*katB*) and a possible homologue (*PSHAa1737*) (Médigue et al.,
749 2005).

750 Furthermore, in order to prevent significant damage to cellular structures, *Ph*TAC125
751 improves the redox buffering capacity of the cytoplasm, and glutathione synthetase is strongly up-
752 regulated at low temperature (Piette et al., 2010). These adjustments in antioxidant defenses are
753 needed to maintain the steady-state concentration of ROS and may be important components in
754 evolutionary adaptations in cold and O_2-rich environments. In fact, *Ph*TAC125 is able to thrive in
755 pelagic form, where cells experience a high concentration of O_2 and other gases that characterise
756 cold waters. In addition, although the strain thrives between 2 and 4 °C, it is also able to survive
757 long-term frozen conditions when entrapped in the winter sea ice (Médigue et al., 2005).

758 The presence of multiple globin genes in distinct positions on chromosome I of *Ph*TAC125
759 (Giordano et al., 2007) may be pivotal for cell protection. To our knowledge, *Ph*TAC125 is the first
760 example of coexistence of genes encoding a FHb and three 2/2Hbs (Giordano et al., 2013), of which

761 both *Ph*-2/2HbO-0030 and *Ph*-2/2HbO-2217 are endowed with hexa-coordination (Giordano et al.,
762 2011; Howes et al., 2011; Russo et al., 2013; Giordano et al., 2015; this study). Endogenous hexa-
763 coordination may be essential for proteins that function under high levels of oxidative stress
764 (Johnson and Lecomte, 2013).

765 When complementing this study with our earlier work (Coppola et al., 2013), it appears that
766 both *Ph*-2/2HbO-2217 and *Ph*-2/2HbO-0030 provide protection against NO and related reactive
767 species, under aerobic conditions. At first sight, two hexa-coordinated globins capable of
768 performing NO detoxification appear redundant. However, variations in physico-chemical features
769 of the marine environment may require diversified responses, which may be reflected in appropriate
770 modulation of gene expression in this bacterium. Our incomplete knowledge of the physiological
771 role of the two globins, which is probably multifaceted, is another aspect that needs to be
772 considered. For example, the genome of many fish species can express multiple Hbs having similar
773 Bohr and Root effects, which points to apparently similar mechanisms in O_2 binding and release.

774 Transcriptional analysis of the genes encoding globins in *Ph*TAC125 wild type and in the
775 *Ph*TAC125-0030 mutant showed that the transcription of the FHb-encoding gene (*PSHAa2880*)
776 was observed in the *Ph*TAC125-0030 mutant when grown at 4 °C in microaerobiosis (Parrilli et al.,
777 2010). Since the transcription of FHb-encoding genes is linked to globin-mediated NO
778 detoxification (Membrillo-Hernàndez et al., 1999; Mills et al., 2001; Stevanin et al., 2000), the
779 observed FHb-gene expression is suggestive of the occurrence of NO-induced stress intimately
780 correlated to the absence of *Ph*-2/2HbO-0030. Although the *Ph*TAC125 genome contains two
781 additional 2/2Hbs encoding genes, transcribed in all the experimental conditions tested in Parrilli et
782 al. (2010), mutation of the gene encoding *Ph*-2/2HbO-0030 is sufficient to obtain a strain with a
783 clear mutant phenotype. This suggests that the numerous globins in this bacterium are not
784 functionally redundant in *Ph*TAC125 physiology.

785 The high reactivity of the ferric forms of *Ph*-2/2HbO-0030 (Coppola et al., 2013) and *Ph*-
786 2/2HbO-2217 towards peroxynitrite suggests that protection against RNS and ROS is a strong need

787 in the cold Antarctic environment. Low temperatures are known to decrease nitrate uptake among
788 bacteria, and nitrogen is fundamental for bacteria replication and synthesis of proteins.
789 Several procedures were attempted to purify the expressed *Ph*-2/2HbO-2217 to
790 homogeneity, but they were unsuccessful thus precluding the possibility to determine its physico-
791 chemical properties under physiological conditions. Therefore, two *in vivo* and *in vitro* models have
792 been developed to highlight the protective role of *Ph*-2/2HbO-2217 against RNS. However, the
793 nitrosative stress-sensitive *E. coli* is protected from NO by ferrous *Ph*-2/2HbO-2217, which is
794 involved in O_2- and NO-consumption (**Figures 6, 7 and 8**), and ferric *Ph*-2/2HbO-2217 which
795 catalyses *in vitro* peroxynitrite scavenging (**Figure 9**). These results suggest that ferrous and ferric
796 *Ph*-2/2HbO-2217 could be involved in the detoxification of RNS (i.e., NO and peroxynitrite,
797 respectively), thus protecting the bacterium from these nitrosative stress mechanisms.
798 The main features of *Ph*-2/2HbO-2217 and *Ph*-2/2HbO-0030 are the presence of a longer
799 sequence extension of the *N*-terminal region (19 residues in *Ph*-2/2HbO-0030 and 9 residues in *Ph*-
800 2/2HbO-2217), that in *Ph*-2/2HbO-0030 is proteolytically cleaved during protein purification
801 (Giordano et al., 2007), and does not appear to reduce the NO scavenging activity (Coppola et al.,
802 2013). Pesce et al. (2016) have recently demonstrated that removal of the pre-A region in *M.*
803 *tuberculosis Mt*-2/2HbN promotes the assembly of a stable dimer, both in the crystals and in
804 solution, hypothesising that the pre-A region may be essential for survival of the microorganism
805 because it significantly reduces the ability of *Mt*-2/2HbN to scavenge NO by interfering with ligand
806 diffusion. Accordingly, kinetic measurements of *Mt*-2/2HbN-DpreA indicate that the k_{on} values for
807 peroxynitrite isomerisation by the mutant protein were four-fold lower than in the wild-type protein
808 (Pesce et al., 2016).
809 Interestingly, also 2/2HbI, encoded by the *PSHAa0458* gene in the *Ph*TAC125 genome, is
810 characterised by an extension at the *N* terminus longer than that observed in *Mt*-2/2HbN; from
811 preliminary results, the protein shows endogenous hexa-coordination (Daniela Giordano, personal
812 communication), similar to the other genes of 2/2Hbs present in the genome of *Ph*TAC125.

Although transcriptional regulation is the main mechanism in stress responses, regulation of translation is faster and consequently very important for species. Post-transcriptional regulation occurs at different stages and includes generation of proteins that need to be activated to perform their function (Varshavsky, 2011). The strategy allows cells to respond quickly to environmental stimuli by simply activating preexistent proteins. We cannot exclude that these extensions at the *N* terminus may play a role in the native host, namely the Antarctic bacterium, although the experiments performed by Coppola et al. (2013) in the mutant of *E. coli* as heterologous host did not show any involvement of the pre-A region of *Ph*-2/2HbO-0030 in NO detoxification. Altogether, these findings indicate the need of *Ph*TAC125 to quickly react to the environment by implementing proteins that function under high levels of oxidative stress.

Acknowledgements

This study is in the framework of the SCAR programme "Antarctic Thresholds - Ecosystem Resilience and Adaptation" (AnT-ERA). It was financially supported by the Italian National Programme for Antarctic Research (PNRA). We are grateful to two anonymous Reviewers, whose comments and suggestions greatly helped us to improve the quality of this paper.

References

Arnold K, Bordoli L, Kopp J, Schwede T (2006) The SWISS-MODEL workspace: a web-based environment for protein structure homology modelling. Bioinformatics, 22, 195-201.

Ascenzi P, Fasano M (2007) Abacavir modulates peroxynitrite-mediated oxidation of ferrous nitrosylated human serum heme-albumin. Biochem. Biophys. Res. Commun. 353, 469-474.

Ascenzi P, De Marinis E, Visca P, Ciaccio C, Coletta M (2009) Peroxynitrite detoxification by ferryl *Mycobacterium leprae* truncated hemoglobin O. Biochem. Biophys. Res. Commun. 380, 392-6.

Ascenzi P, Ciaccio C, Sinibaldi F, Santucci R, Coletta M (2011a) Cardiolipin modulates allosterically peroxynitrite detoxification by horse heart cytochrome *c*. Biochem. Biophys. Res. Commun. 404, 190-194.

Ascenzi P, Ciaccio C, Sinibaldi F, Santucci R, Coletta M (2011b) Peroxynitrite detoxification by horse heart carboxymethylated cytochrome *c* is allosterically modulated by cardiolipin. Biochem. Biophys. Res. Commun. 415, 463-467.

Ascenzi P, di Masi A, Tundo GR, Pesce A, Visca P, Coletta M (2014) Nitrosylation mechanisms of *Mycobacterium tuberculosis* and *Campylobacter jejuni* truncated hemoglobins N, O, and P. PLoS One. 9, e102811.

Benkert P, Biasini M, Schwede T (2011) Toward the estimation of the absolute quality of individual protein structure models. Bioinformatics, 27, 343-350.

Biasini M, Bienert S, Waterhouse A, Arnold K, Studer G, Schmidt T, Kiefer F, Gallo Cassarino T, Bertoni M, Bordoli L, Schwede T (2014) SWISS-MODEL: modelling protein tertiary and quaternary structure using evolutionary information. Nucleic Acids Res. 42: W252-8.

Bohle DS, Glassbrenner PA, Hansert B (1996) Syntheses of pure tetramethylammonium peroxynitrite. Methods Enzymol. 269, 302-311.

858 Bonamore A, Ilari A, Giangiacomo L, Bellelli A, Morea V, Boffi A (2005) A novel thermostable
859 hemoglobin from the actinobacterium *Thermobifida fusca*. FEBS J. 272, 4189-4201.
860 Boubeta FM, Bari SE, Estrin DA, Boechi L (2016) Access and binding of H_2S to hemeproteins: the
861 case of HbI of *Lucina pectinata*. J. Phys. Chem. B. 120, 9642-9653.
862 Bowman LA, McLean S, Poole RK, Fukuto J (2011) The diversity of microbial responses to nitric
863 oxide and agents of nitrosative stress: close cousins but not identical twins. Adv. Microb.
864 Physiol. 59, 135–219.
865 Bustamante JP, Radusky L, Boechi L, Estrin DA, Ten Have A, Martí MA (2016) Evolutionary and
866 functional relationships in the truncated hemoglobin family. PLoS Comput. _
867 Cerda-Còlon JF, Silfa E, Lopez-Garriga J (1998) Unusual rocking freedom of the heme in the
868 hydrogen sulfide-binding hemoglobin from *Lucina pectinata*. J. Am. Chem. Soc. 120, 9312-
869 9317.
870 Ciaccio C, Tognaccini L, Battista T, Cervelli M, Howes BD, Santucci R, Coletta M, Mariottini P,
871 Smulevich G, Fiorucci L (2017) The Met80Ala and Tyr67His/Met80Ala mutants of human
872 cytochrome *c* shed light on the reciprocal role of Met80 and Tyr67 in regulating ligand access
873 into the heme pocket. J. Inorg. Biochem. 169, 86-96.
874 Coppola D, Giordano D, Tinajero-Trejo M, di Prisco G, Ascenzi P, Poole RK, Verde C (2013)
875 Antarctic bacterial hemoglobin and its role in the protection against nitrogen reactive species.
876 Biochim. Biophys. Acta. 1834, 1923-1931.
877 Crowe SA, Døssing LN, Beukes NJ, Bau M, Kruger SJ, Frei R, Canfield DE (2013) Atmospheric
878 oxygenation three billion years ago. Nature. 501, 535-538.
879 De Marinis E, Casella L, Ciaccio C, Coletta M, Visca P, Ascenzi P (2009) Catalytic peroxidation of
880 nitrogen monoxide and peroxynitrite by globins. IUBMB Life. 61, 62-73.
881 Egawa T, Yeh SR (2005) Structural and functional properties of hemoglobins from unicellular
882 organisms as revealed by resonance Raman spectroscopy. J. Inorg. Biochem. 99, 72-96.

883 Feis A, Marzocchi MP, Paoli M, Smulevich G (1994) Spin state and axial ligand bonding in the
884 hydroxide complexes of metmyoglobin, methemoglobin, and horseradish peroxidase at room
885 and low temperatures. Biochemistry. 33, 4577-4583.
886 Gardner PR, Gardner AM, Martin LA, Salzman AL (1998) Nitric oxide dioxygenase: an enzymic
887 function for flavohemoglobin. Proc. Natl. Acad. Sci. USA. 95, 10378–10383.
888 Gardner PR (2005) Nitric oxide dioxygenase function and mechanism of flavohemoglobin,
889 hemoglobin, myoglobin and their associated reductases. J. Inorg. Biochem. 99, 247-266.
890 Giangiacomo A, Ilari L, Boffi A, Morea V, Chiancone E (2005) The truncated oxygen-avid
891 hemoglobin from *Bacillus subtilis*: X-ray structure and ligand binding properties. J. Biol.
892 Chem. 280, 9192-9202.
893 Giordano D, Parrilli E, Dettaï A, Russo R, Barbiero G, Marino G, Lecointre G, di Prisco G, Tutino
894 ML, Verde C (2007) The truncated hemoglobins in the Antarctic psychrophilic bacterium
895 *Pseudoalteromonas haloplanktis* TAC125. Gene. 398, 69-77.
896 Giordano D, Russo R, Ciaccio C, Howes BD, di Prisco G, Marden MC, Hui Bon Hoa G, Smulevich
897 G, Coletta M, Verde C (2011) Ligand- and proton-linked conformational changes of the
898 ferrous 2/2 hemoglobin of *Pseudoalteromonas haloplanktis* TAC125. IUBMB Life. 63, 566-
899 573.
900 Giordano D, Coppola D, Russo R, Tinajero-Trejo M, di Prisco G, Lauro F, Ascenzi P, Verde C
901 (2013) The globins of cold-adapted *Pseudoalteromonas haloplanktis* TAC125: from the
902 structure to the physiological functions. Adv. Microb. Physiol. 63, 329-389.
903 Giordano D, Pesce A, Boechi L, Bustamante JP, Caldelli E, Howes BD, Riccio A, di Prisco G,
904 Nardini M, Estrin D, Smulevich G, Bolognesi M, Verde C (2015) Structural flexibility of the
905 heme cavity in the cold adapted truncated hemoglobin from the Antarctic marine bacterium
906 *Pseudoalteromonas haloplanktis* TAC125. FEBS J. 282, 2948-2965.

907 Giovannoni SJ, Tripp HJ, Givan S, Podar M, Vergin KL, Baptista D, Bibbs L, Eads J, Richardson
908 TH, Noordewier M, Rappé MS, Short JM, Carrington JC, Mathur EJ (2005) Genome
909 streamlining in a cosmopolitan oceanic bacterium. Science. 309, 1242-1245.
910 Goldstein S, Merényi G (2008) The chemistry of peroxynitrite: implications for biological activity.
911 Methods Enzymol. 436, 49-61.
912 Jarboe LR, Hyduke DR, Tran LM, Chou KJ, Liao JC (2008) Determination of the *Escherichia coli*
913 *S*-nitrosoglutathione response network using integrated biochemical and systems analysis. J.
914 Biol. Chem. 283, 5148-5157.
915 Johnson EA, Lecomte JT (2013) The globins of cyanobacteria and algae. Adv. Microb. Physiol. 63,
916 195-272.
917 Hart TW (1985) Some observations concerning the S-nitroso and S-phenylsulphonyl derivatives of
918 L-cysteine and glutathione. Tetrahedron Lett. 26, 2013-2016.
919 Herold S, Shivashankar K (2003) Metmyoglobin and methemoglobin catalyze the isomerization of
920 peroxynitrite to nitrate. Biochemistry. 42, 14036-14046.
921 Herold S, Kalinga S, Matsui T, Watanabe Y (2004a) Mechanistic studies of the isomerization of
922 peroxynitrite to nitrate catalyzed by distal histidine metmyoglobin mutants. J. Am. Chem. Soc.
923 126, 6945-6955.
924 Herold S, Fago A, Weber RE, Dewilde S, Moens L (2004b) Reactivity studies of the Fe(III) and
925 Fe(II)NO forms of human neuroglobin reveal a potential role against oxidative stress. J. Biol.
926 Chem. 279, 22841-22847.
927 Herold S, Fago A (2005) Reactions of peroxynitrite with globin proteins and their possible
928 physiological role. Comp Biochem Physiol A Mol Integr Physiol. 142, 124-129
929 Howes BD, Giordano D, Boechi L, Russo R, Mucciacciaro S, Ciaccio C, Sinibaldi F, Fittipaldi M,
930 Martí MA, Estrin DA, di Prisco G, Coletta M, Verde C, Smulevich G (2011) The peculiar
931 heme pocket of the 2/2 hemoglobin of cold adapted *Pseudoalteromonas haloplanktis* TAC125.
932 J. Biol. Inorg. Chemistry. 16, 299-311.

933 Howes BD, Boechi L, Boffi A, Estrin DA, Smulevich G (2015) Bridging theory and experiment to
934 address structural properties of truncated haemoglobins: Insights from *Thermobifida fusca*
935 HbO. In Adv. Microb. Physiol. Recent Advances in Microbial Oxygen-binding Proteins
936 (Poole RK, Ed.) Vol. 67, 85-126.
937 Kalnenieks U, Galinina N, Kalnenieks U, Galinina N, Bringer- Meyer S, Poole RK (1998)
938 Membrane D-lactate oxidase in *Zymomonas mobilis*: evidence for a branched respiratory
939 chain. FEMS Microbiol. Lett. 168, 91–97.
940 Koppenol WH, Kissner R, Beckman JS (1996) Syntheses of peroxynitrite: to go with the flow or on
941 solid grounds? Methods Enzymol. 269, 296-302.
942 Ilari A, Kjelgaard P, von Wachenfeldt C, Catacchio B, Chiancone E, Boffi A (2007) Crystal
943 structure and ligand binding properties of the truncated hemoglobin from *Geobacillus*
944 *stearothermophilus*. Arch. Biochem. Biophys. 457, 85-94.
945 Laver JR, McLean S, Bowman LA, Harrison LJ, Read RC, Poole RK (2012) Nitrosothiols in
946 bacterial pathogens and pathogenesis. Antioxid. Redox Signal. 18, 309-322.
947 Markwell MA, Haas SM, Bieber LL, Tolbert NE (1978) A modification of the Lowry procedure to
948 simplify protein determination in membrane and lipoprotein samples. Anal. Biochem. 87, 206-
949 210.
950 Marzocchi MP, Smulevich G (2003) Relationship between heme vinyl conformation and the protein
951 matrix in peroxidases. J. Raman Spectrosc. 34, 725-736.
952 Médigue C, Krin E, Pascal G, Barbe V, Bernsel A, Bertin PN, Cheung F, Cruveiller S, D'Amico S,
953 Duilio A, Fang G, Feller G, Ho C, Mangenot S, Marino G, Nilsson J, Parrilli E, Rocha EP,
954 Rouy Z, Sekowska A, Tutino ML, Vallenet D, von Heijne G, Danchin A (2005) Coping with
955 cold: the genome of the versatile marine Antarctica bacterium *Pseudoalteromonas*
956 *haloplanktis* TAC125. Genome Res. 15, 1325-1335.
957 Membrillo-Hernàndez J, Coopamah MD, Anjum MF, Stevanin TM, Kelly A, Hughes MN, Poole
958 RK (1999) The flavohemoglobin of *Escherichia coli* confers resistance to a nitrosating agent,

959 a “nitric oxide releaser”, and paraquat and is essential for transcriptional responses to
960 oxidative stress. J. Biol. Chem. 274, 748-754.
961 Methé BA, Nelson KE, Deming JW, Momen B, Melamud E, Zhang X, Moult J, Madupu R, Nelson
962 WC, Dodson RJ, Brinkac LM, Daugherty SC, Durkin AS, DeBoy RT, Kolonay JF, Sullivan
963 SA, Zhou L, Davidsen TM, Wu M, Huston AL, Lewis M, Weaver B, Weidman JF, Khouri H,
964 Utterback TR, Feldblyum TV, Fraser CM (2005) The psychrophilic lifestyle as revealed by the
965 genome sequence of *Colwellia psychrerythraea* 34H through genomic and proteomic analyses.
966 Proc. Nati. Acad. Sci. USA. 102, 10913-10918.
967 Milani M, Savard PY, Ouellet H, Ascenzi P, Guertin M, Bolognesi M (2003) A TyrCD1/TrpG8
968 hydrogen bond network and a TyrB10TyrCD1 covalent link shape the heme distal site of
969 *Mycobacterium tuberculosis* hemoglobin O. Proc Natl Acad Sci USA. 100, 5766–5771.
970 Milani M, Pesce A, Nardini M, Ouellet H, Ouellet Y, Dewilde S, Bocedi A, Ascenzi P, Guertin M,
971 Moens L, Friedman JM, Wittenberg JB, Bolognesi M (2005) Structural bases for heme
972 binding and diatomic ligand recognition in truncated hemoglobins. J. Inorg. Biochem. 99, 97-
973 109.
974 Mills CE, Sedelnikova S, Søballe B, Hughes MN, Poole RK (2001) *Escherichia coli*
975 flavohaemoglobin (Hmp) with equistoichiometric FAD and haem contents has a low affinity
976 for dioxygen in the absence or presence of nitric oxide. Biochem. J. 353, 207-213.
977 Nardini M, Pesce A, Milani M, Bolognesi M (2007) Protein fold and structure in the truncated (2/2)
978 globin family. Gene. 398, 2-11.
979 Nicoletti FP, Bustamante JP, Droghetti E, Howes BD, Fittipaldi M, Bonamore A, Baiocco P, Feis
980 A, Boffi A, Estrin DA, Smulevich G (2014) Interplay of the H-bond donor−acceptor role of
981 the distal residues in hydroxyl ligand stabilization of *Thermobifida fusca* truncated
982 hemoglobin. Biochemistry. 53, 8021-8030.

983 Parrilli E, Giuliani M, Giordano D, Russo R, Marino G, Verde C, Tutino ML (2010) The role of a
984 2-on-2 haemoglobin in oxidative and nitrosative stress resistance of Antarctic
985 *Pseudoalteromonas haloplanktis* TAC125. Biochimie. 92, 1003-1009.
986 Pesce A, Nardini M, Labarre M, Richard C, Wittenberg JB, Wittenberg BA, Guertin M, Bolognesi
987 M (2011) Structural characterization of a group II 2/2 hemoglobin from the plant pathogen
988 *Agrobacterium tumefaciens*. Biochim. Biophys. Acta. 1814, 810-816.
989 Pesce A, Bolognesi M, Nardini M (2013) The diversity of 2/2 (truncated) globins. Adv. Microb.
990 Physiol. 63, 49-78.
991 Pesce A, Bustamante JP, Bidon-Chanal A, Boechi L, Estrin DA, Luque FJ, Sebilo A, Guertin M,
992 Bolognesi M, Ascenzi P, Nardini M (2016) The N-terminal pre-A region of *Mycobacterium*
993 *tuberculosis* 2/2HbN promotes NO-dioxygenase activity. FEBS J. 283, 305-322.
994 Piette F, D'Amico S, Struvay C, Mazzucchelli G, Renaut J, Tutino ML, Danchin A, Leprince P,
995 Feller G (2010) Proteomics of life at low temperatures: trigger factor is the primary chaperone
996 in the Antarctic bacterium *Pseudoalteromonas haloplanktis* TAC125. Mol. Microbiol. 76,
997 120-132.
998 Rabus R, Ruepp A, Frickey T, Rattei T, Fartmann B, Stark M, Bauer M, Zibat A, Lombardot T,
999 Becker I, Amann J, Gellner K, Teeling H, Leuschner WD, Glöckner FO, Lupas AN, Amann
1000 R, Klenk HP (2004) The genome of *Desulfotalea psychrophila*, a sulfate-reducing bacterium
1001 from permanently cold Arctic sediments. Environ. Microbiol. 6, 887-902.
1002 Russo R, Giordano D, di Prisco G, Hui Bon Hoa G, Marden MC, Verde C, Kiger L (2013) Ligand
1003 rebinding kinetics of 2/2 hemoglobin from the Antarctic bacterium *Pseudoalteromonas*
1004 *haloplanktis* TAC125. Biochim. Biophys. Acta. 1834, 1932-1938.
1005 Smulevich G, Hu S, Rodgers KR, Goodin DB, Smith KM, Spiro TG (1996) Heme-protein
1006 interactions in CCP revealed by site-directed mutagenesis and Resonance Raman spectra of
1007 isotopically labeled hemes. Biospectroscopy 2, 365-376.

1008 Stevanin TM, Ioannidis N, Mills CE, Kim SO, Hughes MN, Poole RK (2000) Flavohemoglobin
1009 Hmp affords inducible protection for *Escherichia coli* respiration, catalyzed by cytochromes
1010 bo' or bd, from nitric oxide. J. Biol. Chem. 275, 35868-35875.
1011 Vasudevan SG, Armarego WL, Shaw DC, Lilley PE, Dixon NE, Poole RK (1991) Isolation and
1012 nucleotide sequence of the *hmp* gene that encodes a haemoglobin-like protein in *Escherichia*
1013 *coli* K-12. Mol. Gen. Genet. 226, 49-58.
1014 Visca P, Fabozzi G, Petrucca A, Ciaccio C, Coletta M, De Sanctis G, Bolognesi M, Milani M,
1015 Ascenzi P (2002) The truncated hemoglobin from *Mycobacterium leprae*. Biochem. Biophys.
1016 Res. Commun. 294, 1064-1070.
1017 Vinogradov SN, Hoogewijs D, Bailly X, Arredondo-Peter R, Gough J, Dewilde S, Moens L,
1018 Vanfleteren JR (2006) A phylogenomic profile of globins. BMC Evol. Biol. 6, 31.
1019 Vinogradov S, Tinajero-Trejo M, Poole RK, Hoogewijs D (2013) Bacterial and archaeal globins - A
1020 revised perspective. Biochim. Biophys. Acta. 1834, 1789-1800.
1021 Vuletich DA, Lecomte JT (2006) A phylogenetic and structural analysis of truncated hemoglobins.
1022 J. Mol. Evol. 62, 196-210.
1023 Varshavsky A (2011) The N-end rule pathway and regulation by proteolysis. Protein Sci. 20, 1298-
1024 1345.
1025 Wittenberg JB, Bolognesi M, Wittenberg BA, Guertin M (2002) Truncated hemoglobins: A new
1026 family of hemoglobins widely distributed in bacteria, unicellular eukaryotes, and plants. J.
1027 Biol. Chem. 227, 871-874.
1028